Final Technical Report

DESIGN AND DEVELOPMENT OF SOLID STATE DETECTOR FOR SCADS

Contract No. NAS 5-11270

NASA-Goddard Space Flight Center
Greenbelt, Maryland

HONEYWELL
Radiation Center
2 Forbes Road
Lexington, Massachusetts 02173

Final Technical Report

DESIGN AND DEVELOPMENT OF SOLID STATE DETECTOR FOR SCADS

Contract No. NAS 5-11270

NASA-Goddard Space Flight Center
Greenbelt, Maryland

October 1971

HONEYWELL
Radiation Center
2 Forbes Road
Lexington, Massachusetts 02173

TABLE OF CONTENTS

TABLE OF CONTENTS (continued)

SECTION 1

INTRODUCTION

The solid state detector technology developed under Phase I of this contract was applied to the fabrication and testing of cadmium sulfide and silicon narrow slit detector/preamplifier subassemblies. Fabrication of the silicon detector and the cadmium sulfide detectors was accomplished at Honeywell Radiation Center by utilizing cadmium sulfide cells and silicon cells similar to those described and utilized in uniformity testing under Phase I of this contract. Fabrication of the preamplifiers for both silicon and cadmium sulfide slit type detectors was also carried out at Honeywell Radiation Center. The design of these preamplifiers was adjusted to ascertain that the limiting noise source of the detector/preamplifier subassembly is the detector and the input cable.

Not only were the silicon detectors tested individually for: responsivity, uniformity, noise per root cycle, D*, dark leakage current, impedance, active area; but the silicon and cadmium sulfide detector/preamplifier subassemblies were tested at Honeywell Radiation Center by transiting the image of a simulated star, created by a simulated optical subsystem, across the detector slit. Various magnitudes and various transit speeds provided the following information.

1) Star transit with (+3 mag star)

2) S/N vs transit rate

3) Star transit pulse shape measurements

4) Rise time vs star magnitude

By simultaneously displacing the slit orthogonal to the direction of transit, the uniformity and sensitivity of the detectors were also verified.

The three cadmium sulfide and three silicon detectors along with the corresponding preamplifier and detector/preamplifier subassembly test data have been delivered under contract requirements.

SECTION 2

CELL FABRICATION

2.1 CADMIUM SULFIDE

The three cadmium sulfide slit detectors (0.3 mil x 500 mils) incorporated in the encased detector assemblies were constructed at Honeywell Systems and Research Center under Phase I of this contract.

Under Phase II of this contract, these three cadmium sulfide detectors were assembled within a modified cold weld monolithic flat pack header (HC/41U) purchased from GTI Corporation. The header modification is shown in Figure 2.1. The detector glass substrate was bonded over the hole cut in the HC/41U header with glass adhesive manufactured by Adhesive Engineering Company. A microscope glass, cut to the dimensions of the header flanges, was bonded to the flange with glass adhesive, thus forming a vapor seal. The seal was completed in a room environment of approximately 70°F and 35% relative humidity. Contact was established by compression bonding indium to the aluminum substrate. The gold connection lead was then compression bonded into the indium. The gold connection lead was soldered to the steel-kovar header eyelet. An additional equipment ground was provided on the detector case for shield purposes. The preamplifier was connected by a Microdot 202-3932 Twinax shielded cable. The entire cadmium sulfide cell assembly is shown in Figure 2.2.

2.2 SILICON

The three p on n type silicon photovoltaic slit detector assemblies with 2-mil x 500-mil chips, were fabricated at Honeywell Radiation Center. The p on n type silicon was selected over the n on p type silicon because of the superior signal to noise characteristics as demonstrated in the silicon cell fabricated both at Honeywell Radiation Center and Electro-Nuclear Laboratory.

The following describes the fabrication techniques used in the manufacturing of the 3 silicon detectors. The base material used for fabrication was 0.2 ohm-cm N-type silicon of 1,1,1 orientation.

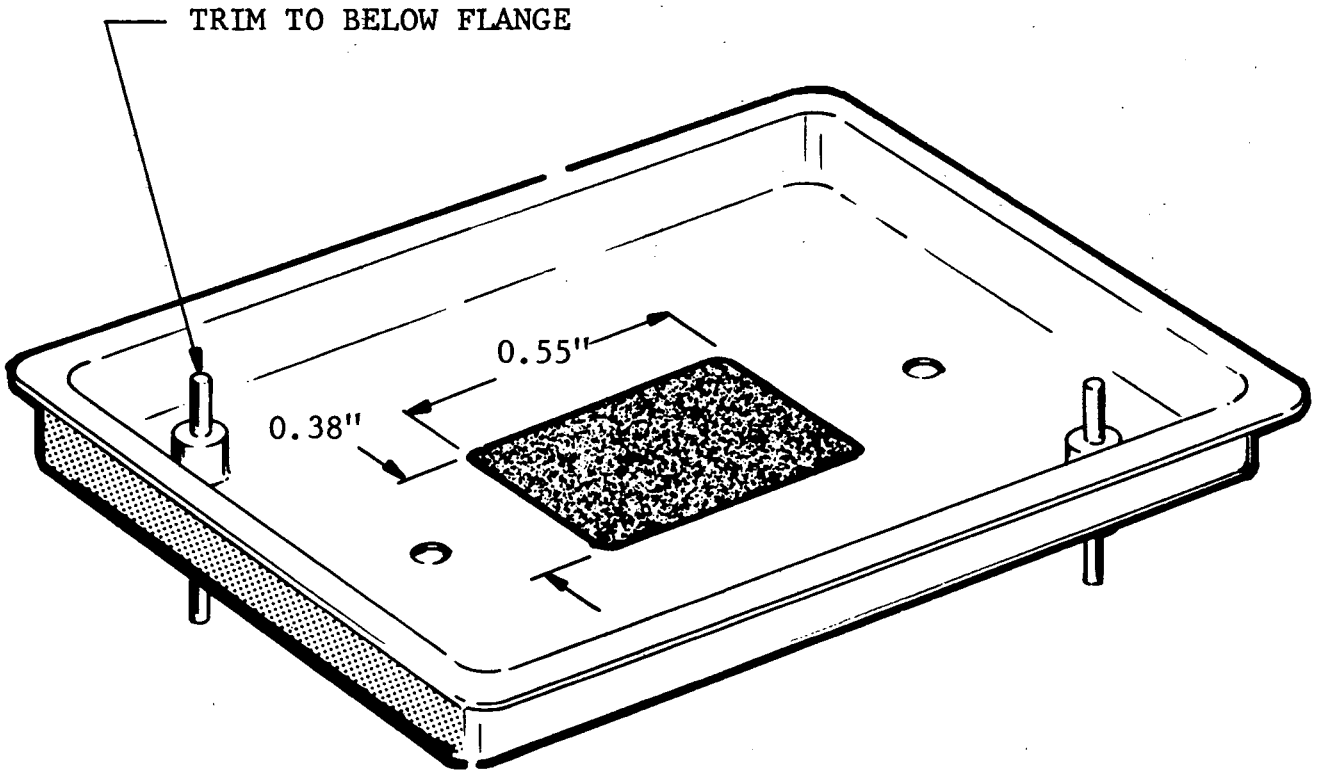

Figure 2.1 ILLUSTRATION OF HC/410 FLAT PACK HEADER

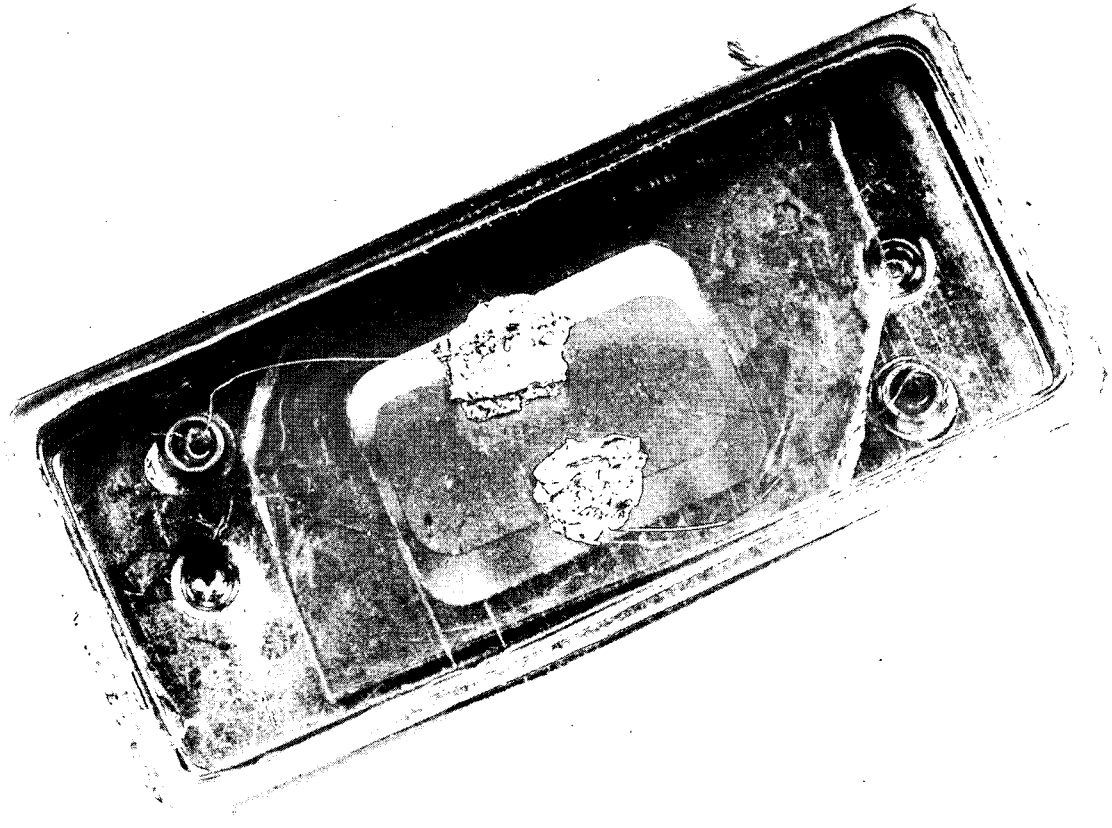

Figure 2.2 CADMIUM SULFIDE CELL ASSEMBLY

A p-type Boron diffusion of approximately 2 mils x 500 mils was carried out on this base material for 60 min. to an estimated depth of 2 microns. An aluminum pad was evaporated on a keyhole shaped area of the end of the slit type p on n junction. To this pad was thermo-compression bonded a 1.0 mil gold lead. The base material was nickel plated and soldered to a double sided copper plated printed circuit board. A 1.0 mil gold lead was also soldered to this surface. The bottom side of the printed circuit board was bonded with glass adhesive to the HC/410 header.

These detector chips were packaged in the containers provided for the cadmium sulfide detector described in Section 2.1 with the following exceptions:

> The container is not modified by cutting out the 0.38 x 0.55 in. rectangular window in the bottom of the container as indicated in Figure 2.1. The window only permitted the back illumination of cadmium sulfide for the purpose of improving response time, a feature which is not required on silicon detectors. The entire silicon cell assembly is shown in Figure 2.3.

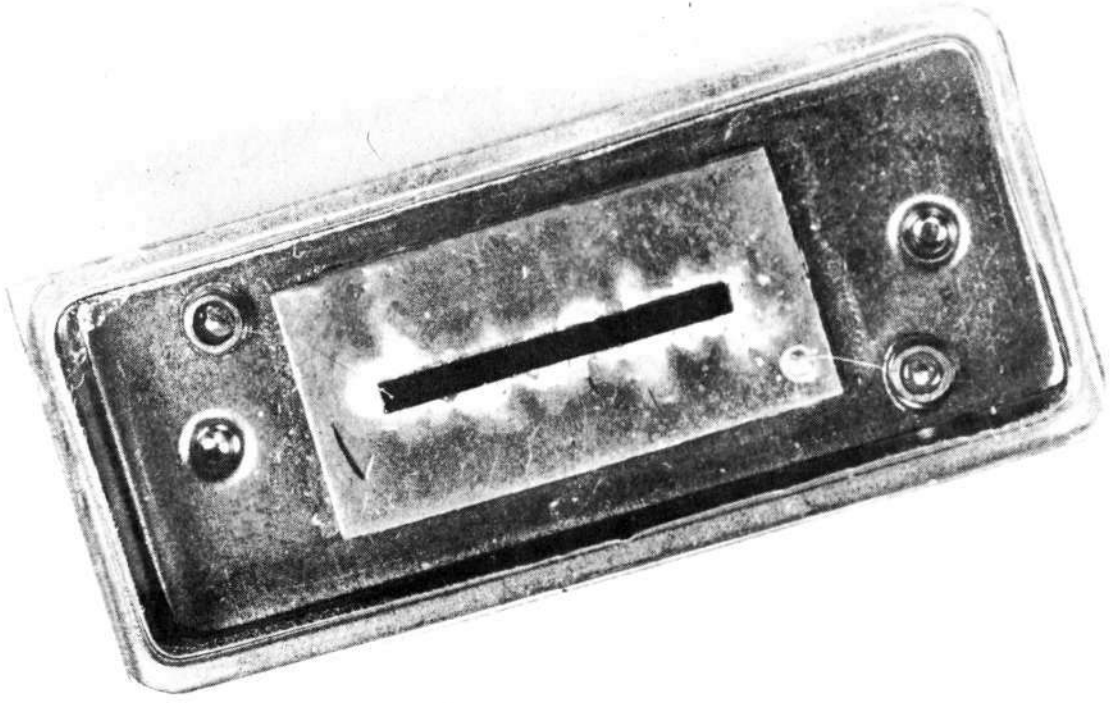

Figure 2.3 SILICON CELL ASSEMBLY

SECTION 3

PREAMPLIFIER FABRICATION

3.1 CADMIUM SULFIDE

3.1.1 Preamplifier Description

The cadmium sulfide preamplifier is a modified version of the Honeywell standard high impedance amplifier. The modifications involved are: 1) the insertion of a biasing network to enable 0.75 volt bias to be applied to the photoresistive type cadmium sulfide detectors, and 2) the insertion of back-to-back diodes in the feedback loop to allow operation on stars that are so bright or star transits that are so slow as to create output voltages that are saturated. The amplifier is an operational type which employs a 100-megohm feedback resistor. Thus, the input is at a virtual ground potential, and the gain in the bandpass region of the preamplifier is approximately 10^8 $\frac{\text{volts output}}{\text{ampere input}}$.

3.1.2 Cadmium Sulfide Preamplifier Measurements

Using the laboratory test set-up shown in Figure 3.1, the following parameters of the cadmium sulfide preamplifier were measured.

Bandpass 3 dB voltage = 0.7 Hz to 57 Hz

For output levels <0.7 volts gain at 7 Hz = 1.05×10^9 V/A for signal less than volts.

It is noted that for output levels >0.7 volts gain at 7 Hz will be equal to 1.05×10^8 V/A.

The noise equivalent inputs were obtained by utilizing the test set-up shown in Figure 3.2.

In Test 1, the preamplifier noise was measured as follows:

$$\text{Preamplifier Noise Equivalent Input} = \frac{2 \text{ mV pk-pk}}{1.05 \times 10^9 \text{ V/A}}$$

$$\left(\frac{1 \text{ rms noise}}{6 \text{ pk-pk noise}}\right) = 0.317 \times 10^{-12} \text{ A rms}$$

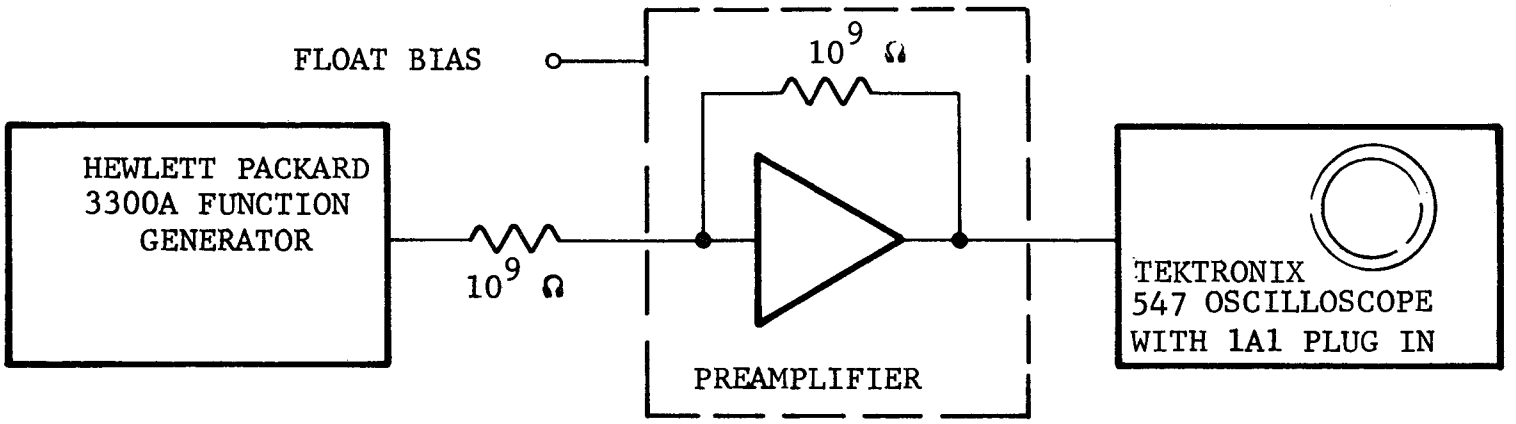

Figure 3.1 PREAMPLIFIER TEST CONFIGURATION "A"

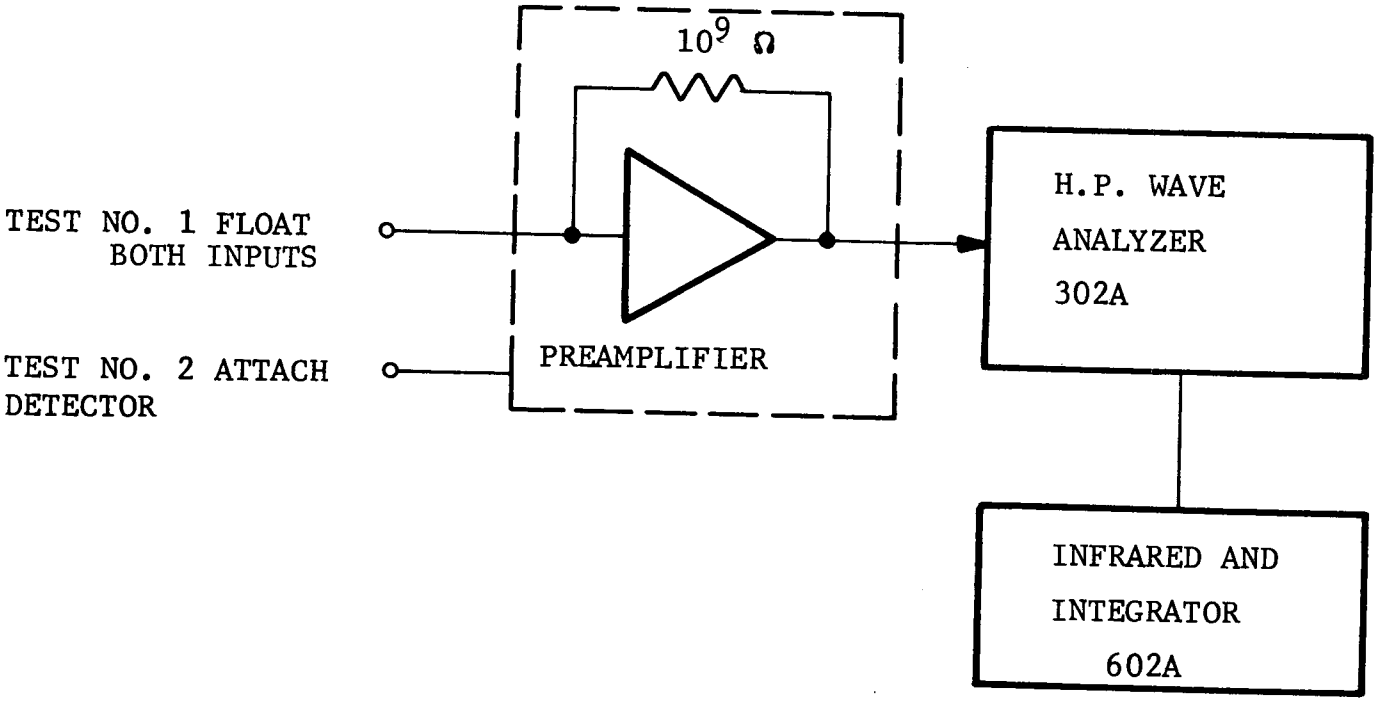

Figure 3.2 PREAMPLIFIER TEST CONFIGURATION "B"

In Test 2, by replacing the resistor with cadmium sulfide cell No. 10 and localizing the cell in total darkness, the following parameter was recorded:

Detector No. 10/Preamplifier Noise Equivalent Input Current =

$$\frac{5 \text{ mV pk-pk}}{1.05 \times 10^{9} \text{ V/A}} \left(\frac{1 \text{ rms noise}}{6 \text{ pk-pk noise}}\right) = .793 \times 10^{-12} \text{ A rms}$$

Amplifier connections are shown in Table 3.1. The cadmium sulfide preamplifier is shown in Figure 3.3.

Table 3.1

CADMIUM SULFIDE AND SILICON PREAMPLIFIER CONNECTIONS

Power Cable	
Amphenol miniature hexagon 9-pin plug no. 220	
Red +15	Pin H
White -15	Pin C
Black ground	Pin E
Brown shield ground	
Power Connector	
Amphenol miniature hexagon 9-pin socket no. 221	
Pin H	+15
Pin C	-15
Pin E	ground
Input Connection	
Microdot Twinax No. 202-4037	
Output Connector	
Amphenol series BNC No. 625 B/U Bulkhead Receptacle	

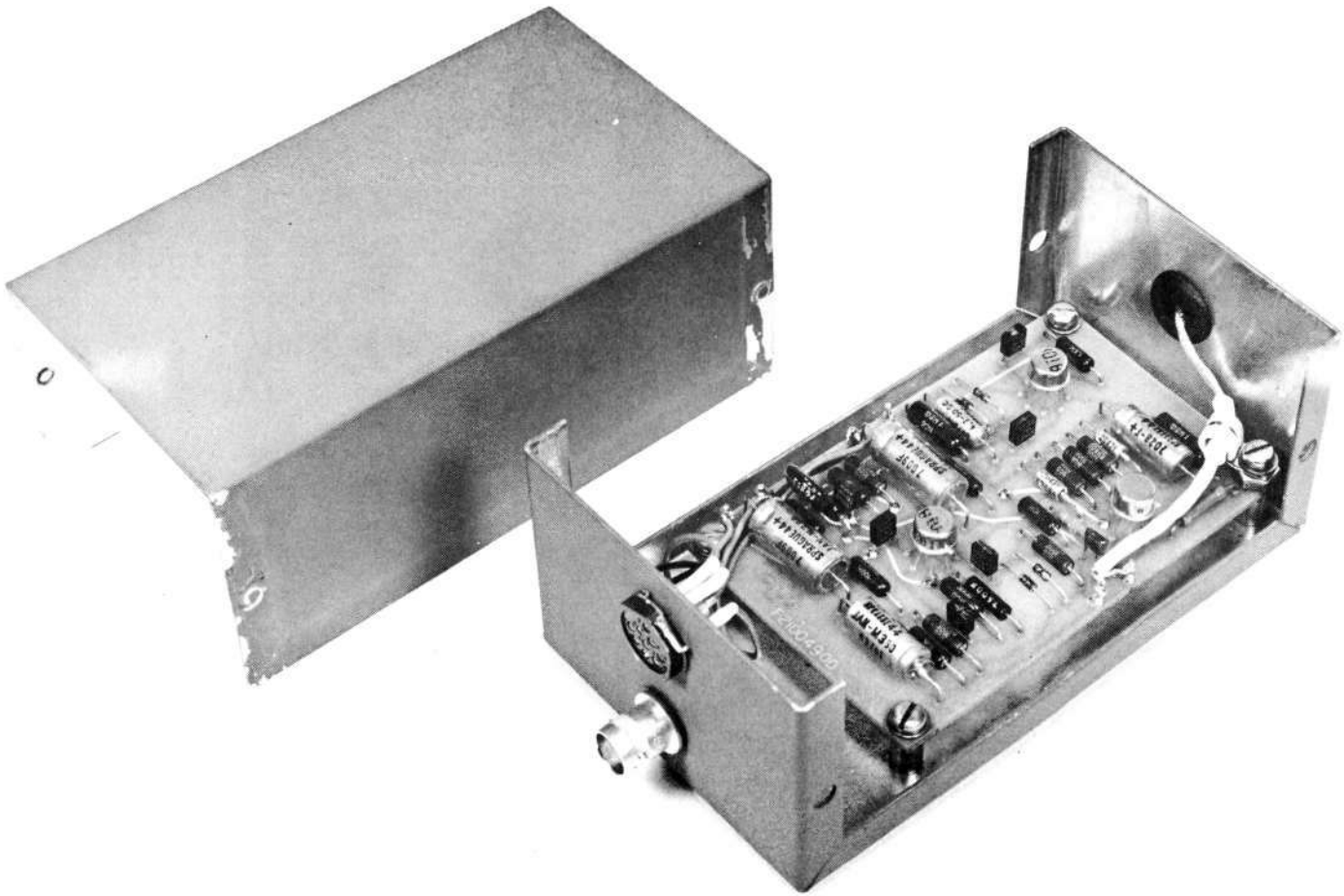

Figure 3.3 CADMIUM SULFIDE PREAMPLIFIER

3.2 SILICON

3.2.1 Preamplifier Description

The silicon preamplifier is a standard Honeywell high impedance amplifier. This amplifier is also an operational type, but it employs a 1000-megohm feedback resistor. Thus, as with cadmium sulfide, the input is at a virtual ground potential, but the gain in the bandpass region of the preamplifier is approximately $10^9 \frac{\text{volt output}}{\text{ampere input}}$

3.2.2 Silicon Preamplifier Measurements

The test set-up used in laboratory measurements of the amplifier parameters, is identical to that used with cadmium sulfide.

The measured parameters are:

Bandpass 3 dB voltage = 0.5 Hz to 580 Hz

Gain at 100 Hz = 1.1×10^9 Volt output/Amp input

Input offset voltage = (-0.4 mV)

Preamplifier Noise Equivalent Input - open input

$$\frac{1 \text{ mV pk-pk}}{1.1 \times 10^9 \text{ V/A}} \left(\frac{1 \text{ rms noise}}{6 \text{ pk-pk noise}}\right) = 0.15 \times 10^{-12} \text{ A rms}$$

Detector/Preamplifier Noise Equivalent Input - Cell No. 1

$$\frac{2 \text{ mV pk-pk}}{1.1 \times 10^9 \text{ V/A}} \left(\frac{1 \text{ rms noise}}{6 \text{ pk-pk noise}}\right) = 0.30 \times 10^{-12} \text{ A rms}$$

Amplifier connections are identical to those shown in Table 3.1 The silicon preamplifier is shown in Figure 3.4.

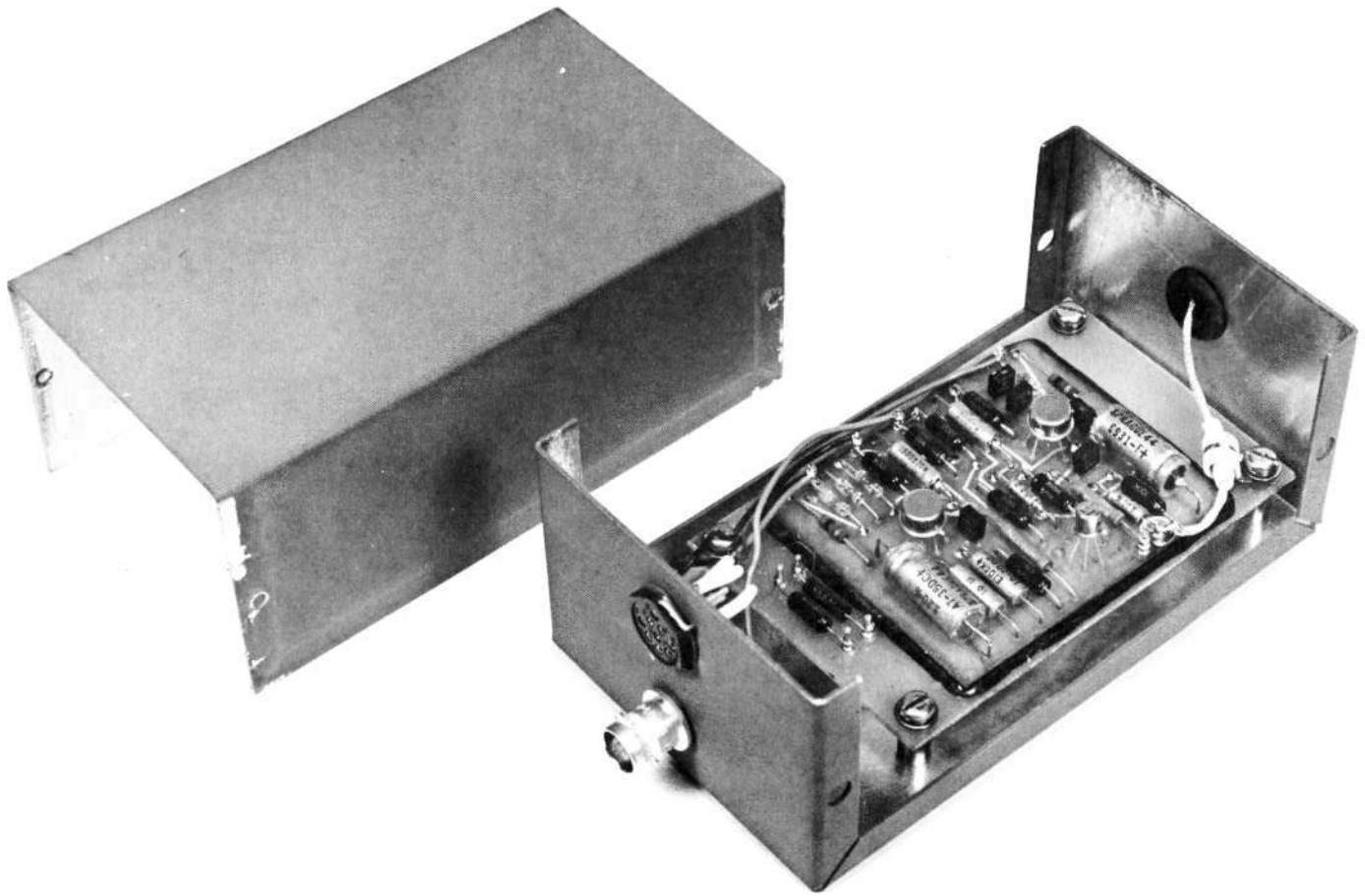

Figure 3.4 SILICON PREAMPLIFIER

SECTION 4

CADMIUM SULFIDE SYSTEM FINAL TESTS

4.1 TEST DESCRIPTION

The apparatus used for testing the cadmium sulfide system is depicted in Figure 4.1. A pinhole is illuminated by imaging a ribbon filament onto it. During this procedure, the required color filter and neutral density filters are inserted to simulate the proper final image intensity and spectral distribution. The pinhole is then imaged by a microscope objective on the surface of the detector. The entire illumination system oscillates in a horizontal plane at a constant speed established by the observer, and thus translates the star image over the detector slit at a specified rate. The detector slit is oriented in a vertical direction and is slowly scanned in an orthogonal vertical plane. Thus, cell uniformity can be verified assuring that whatever spot is picked to perform other transits is truly a spot representative of the performance of the detectors.

The cadmium sulfide cell was background illuminated by a flashlight bulb connected to a battery operated rheostat. The background illumination level is established by increasing the lamp voltage until the peak to peak noise output of the cell is increased to approximately 1.5 times the zero background peak to peak noise output.

Later in the test, the cell impedance was determined by monitoring the voltage created across the feedback resistor (metal film type 10-megohm Victoreen) in the ADC loop of the preamplifier. Since

a) the voltage across the 10-megohm Automatic Drift Compensation (ADC) resistor is known,

b) the steady state input voltage must be zero on the operational amplifier, and

c) the cell has a bias voltage of 0.75 volt imposed across it, the actual cell resistance (R) is

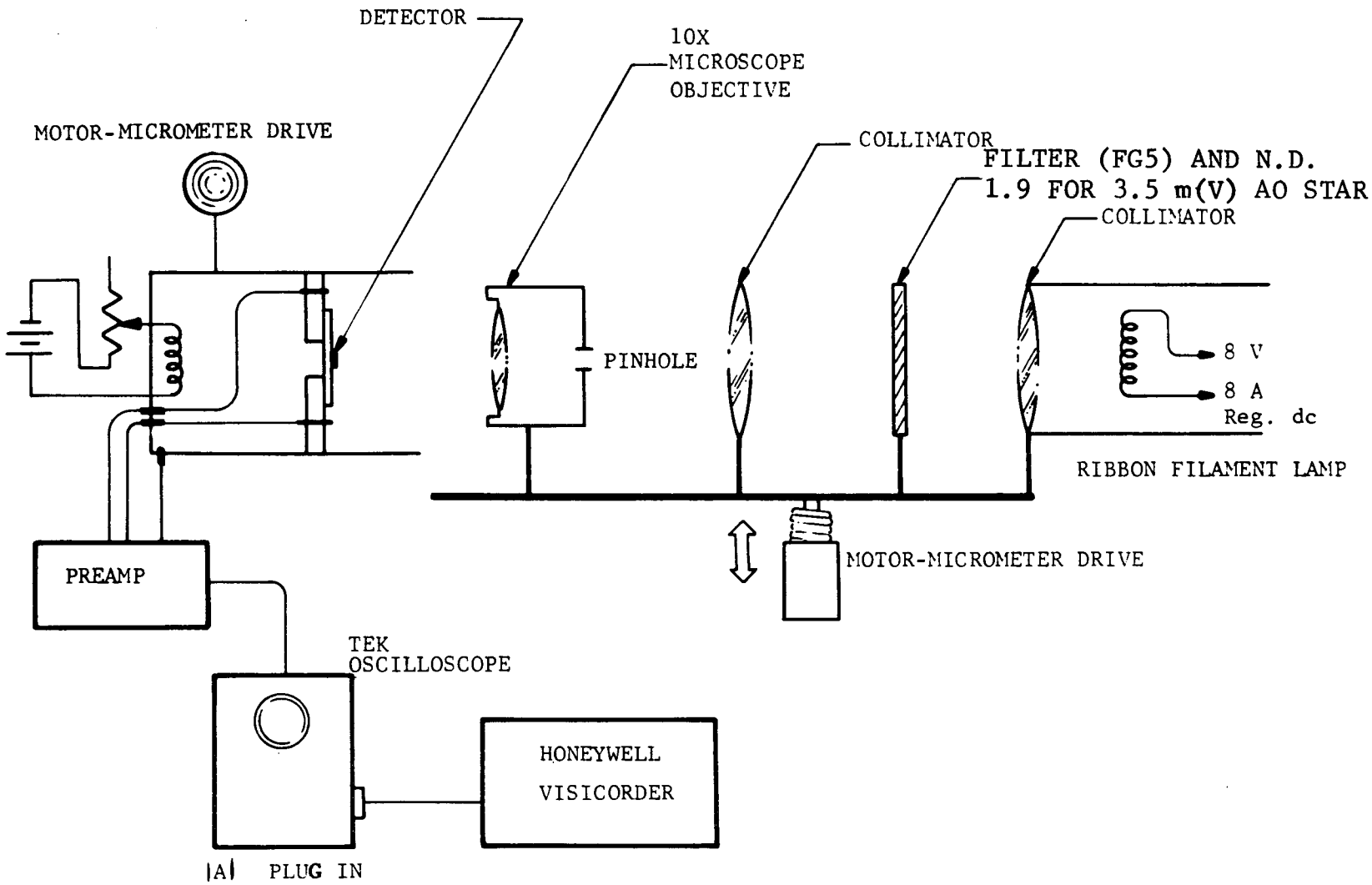

Figure 4.1 CADMIUM SULFIDE SYSTEM TESTS

$$R = \frac{0.75 \text{ volt}}{(\text{ADC voltage created by background})} \times (10 \text{ megohms})$$

The preamplifier was powered by 2 Kepco power supplies, and grounding was highly controlled to eliminate 60-Hz pickup on the cell or the preamplifier.

The intensity of the spot of light transiting the detector was calibrated according to this procedure.

The following assumptions were made regarding a star mapper optical system.

a) The effective collection aperture is 3 inches in diameter.

b) The optical system has a transmission efficiency described by 80% of incident energy focused on a spot approximately 0.25 mil to 0.35 mil in diameter from 0.4 to 0.7 μm.

The HRC translating detector/preamplifier tester focuses an A0 star spectral distribution to a spot of light 0.2 mil in diameter, measured at the first diffraction zone, on a detector as described in Figure 4.1.

By viewing this spot of light with the Spectra Prichard Photometer with the Micro Spectra lens as shown in Figure 4.2, the total luminous flux present at the focused spot can then be established to be identical to theoretical value of luminous flux created by a known Mag star imaged by the theoretical optical system. The results of this comparison are:

a) The theoretical value of luminous flux from a 3.5 m(v) A0 Star is calculated in Appendix E and equals 4.1×10^{-10} lumens.

b) The measured value of luminous flux unattenuated by neutral density filtering but with 5.5 mm of (Jena glass) FG5 filters to simulate an A0 class star is 3.5×10^{-8} lumens as indicated in Appendix F.

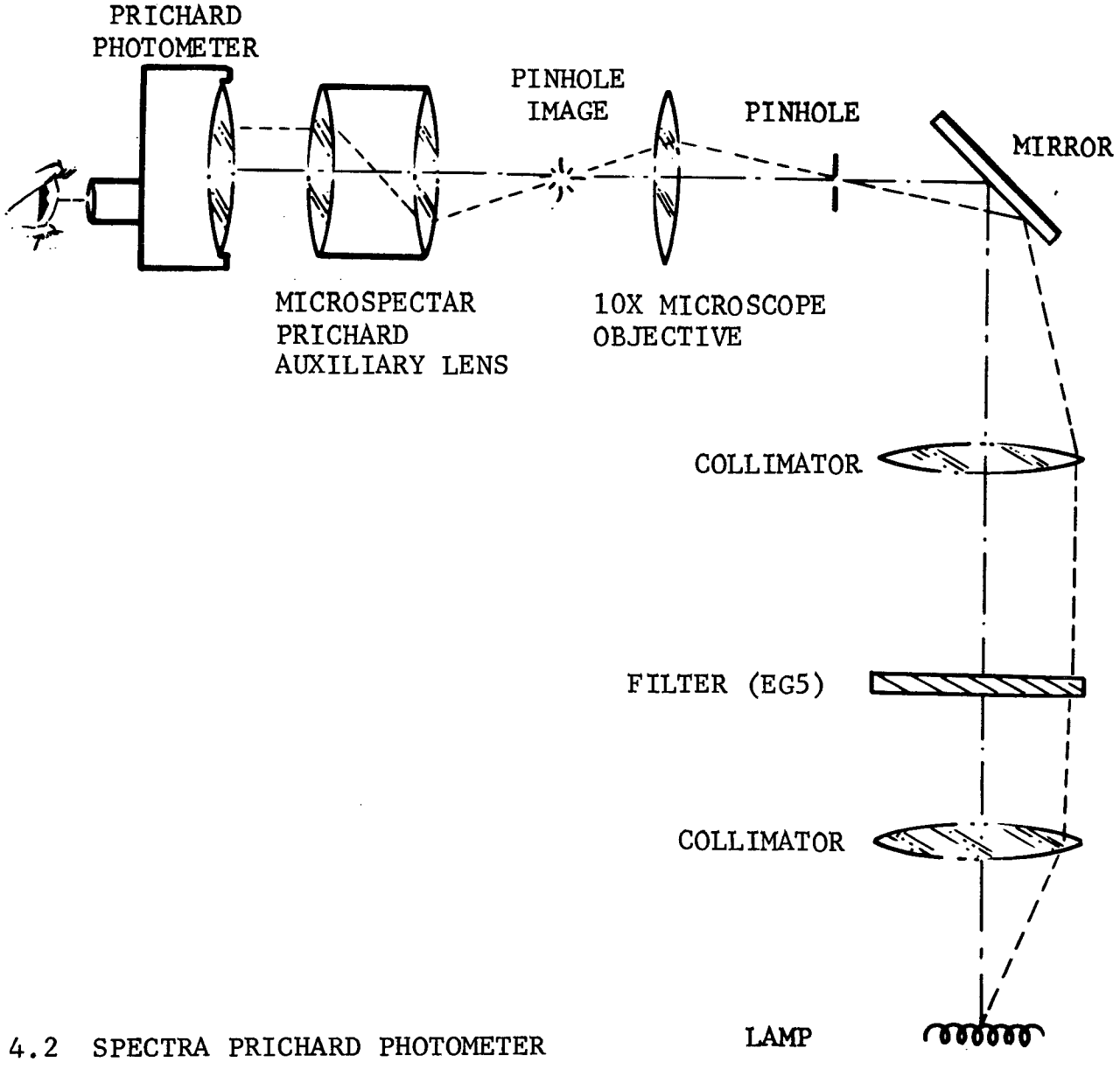

Figure 4.2 SPECTRA PRICHARD PHOTOMETER

A ratio of $3.5 \times 10^{-8}/4.1 \times 10^{-10}$ lumens equals 85.4. The log of 85.4 is 1.93. Thus 1.9 neutral density filtering is required to properly simulate the illumination created by a 3.5 m(v) A0 star imaged by a high quality 3-inch diameter optical system described above.

The output voltage from the preamplifier was displayed on a Taktronix type 547 oscilloscope with a type 1A7A amplifier. When the oscilloscope signal was on scale, the output signal from the 1A7A oscilloscope amplifier is displayed on the Honeywell type 1508A Visicorder with Honeywell Accurata 117 amplifiers. The Visicorder is calibrated for 1 volt/inch sensitivity.

The 1A7A Tektronix Amplifier connected to the Honeywell Visicorder (set at 1 volt/inch sensitivity) was calibrated with known levels of input signals.

The following tests were carried out on cadmium sulfide cells No. 8, 9 and 10.

1) A uniformity scan was recorded at a 10-millisecond transit rate with a +2.75 mag A0 class star and approximately 10 mils displacement between transits over > 0.400 inch of the cell.

2) At a spot selected as being characteristic of the average sensitivity of the cell, the following scans were made.

   a. A 10-millisecond transit with a +2.75 -Mag A0 class star

   b. A 10-millisecond transit with a +1.75 -Mag A0 class star

   c. A 10-millisecond transit with a +0.75 -Mag A0 class star

   d. A 50-millisecond transit with a +2.75 -Mag A0 class star.

4.2 TEST RESULTS

Figures 4.3 through 4.11 show the results of the tests performed as indicated in Section 4.1.

4.2.1 Uniformity

Figures 4.3, 4.6 and 4.9 indicate the uniformity of 10-millisecond star transits with a simulated +2.75 the detector.

The results are:

Cell No.	$\frac{\text{Max Sig-Min Sig}}{\text{Ave Sig}}$	Uniformity
8	$\frac{2x(19-1.5)}{1.5 + 19}$	= ±85% deviation from average response for 93% of transits
9	$\frac{2x(36-11)}{11 + 36}$	= ±53% deviation from average response for 92% of transits
10	$\frac{2x(21-4.5)}{4.5 +21}$	= ±64% deviation from average response for 92% of the transits

Average Uniformity = ±67% deviation from average response for 92% of the transits

4.2.2 Signal to Noise

The relationship between peak to peak noise and rms noise for a white noise spectrum is

(rms noise = $\frac{1}{6}$ peak to peak noise, for less than a 99.8% deviation)

Thus, from Figures 4.4, 4.7 and 4.10, the signal/rms noise ratio for 10-millisecond transit rates on a 2.75 Mag star are:

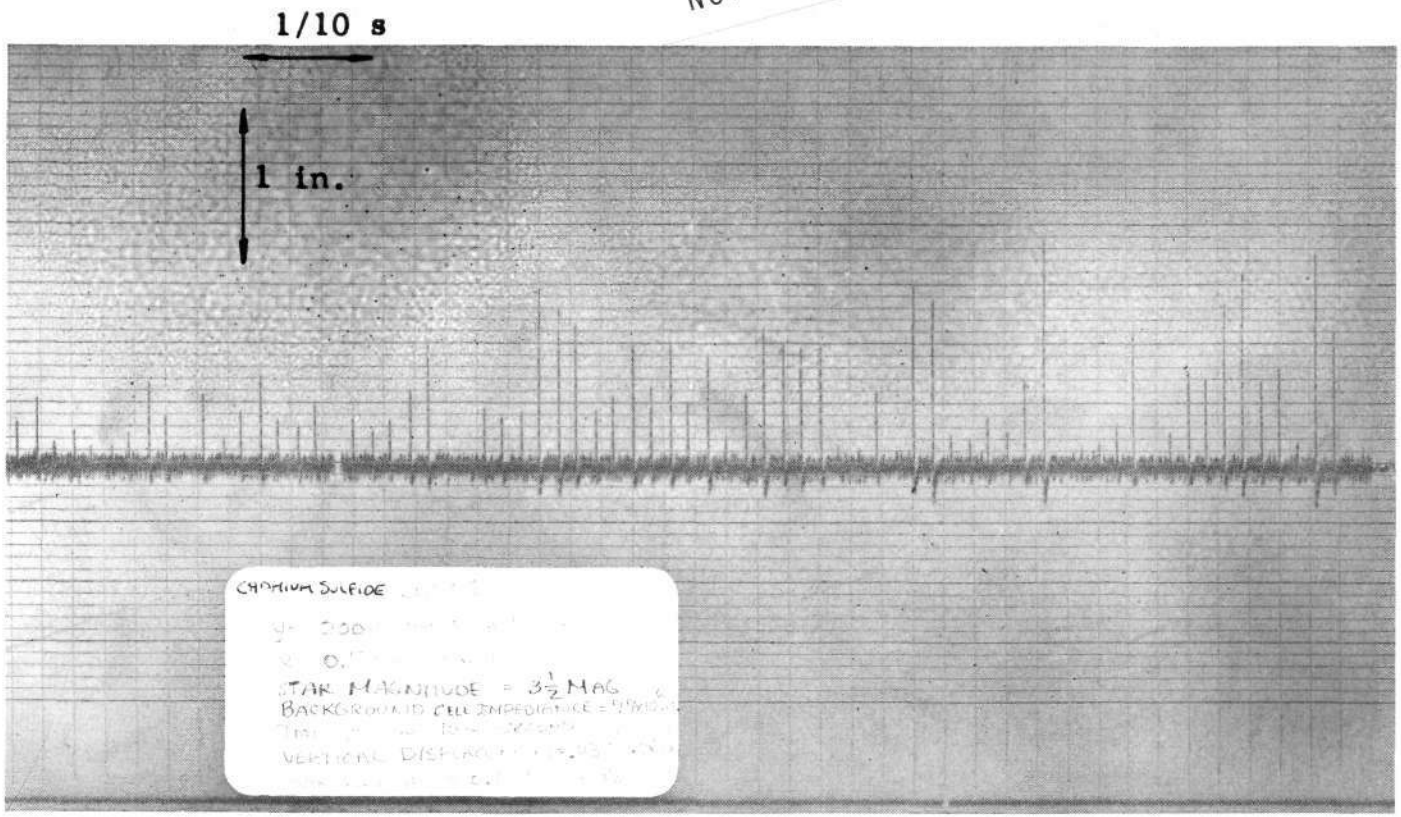

Figure 4.3 CADMIUM SULFIDE CELL NO. 8, y = 200 millivolts/in.; x = 0.5 mm/s; Star Magnitude =+2.75 mag; Background Cell Impedance = 77 x 10^6 Ω; Transit~10 millisecond; Vertical Displacement = .432 in. - .050 in.; Bandwidth = 0.1 to 100 Hz

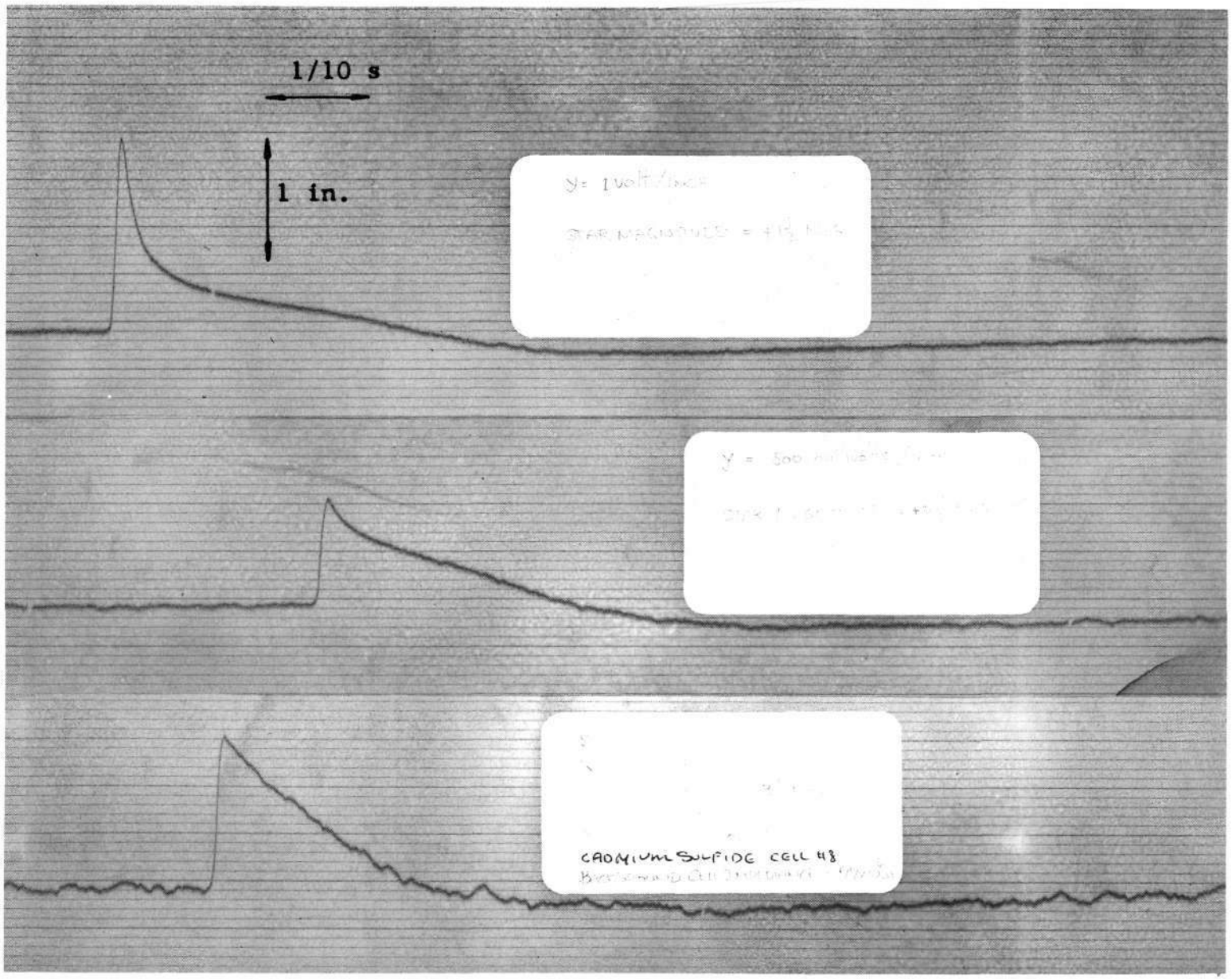

Figure 4.4 CADMIUM SULFIDE CELL NO. 8

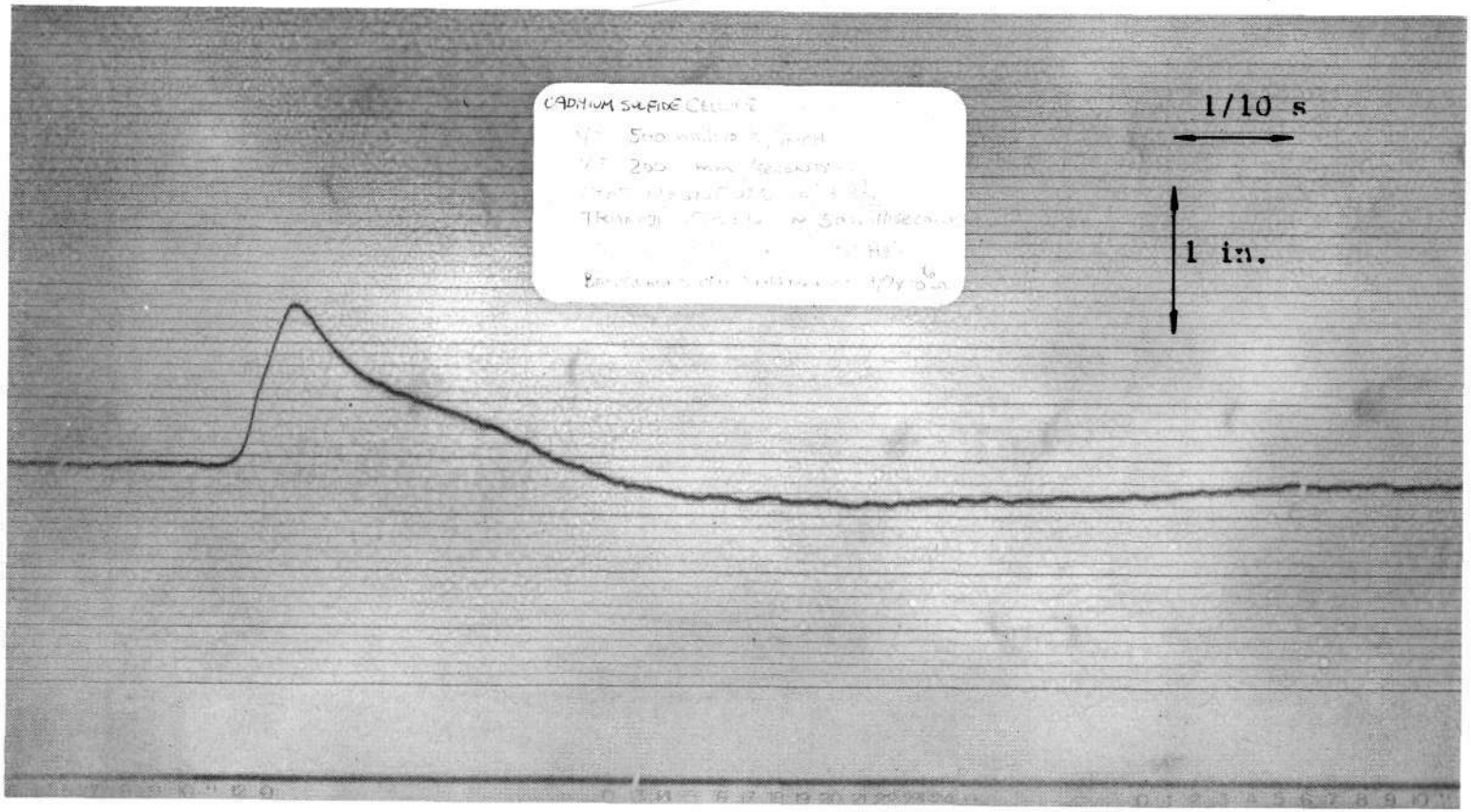

Figure 4.5 CADMIUM SULFIDE CELL NO. 8; y = 500 millivolts/in.; x = 200 mm/s; Star Magnitude = $+2.75$; Transit Speed $\sim$ 50 milliseconds; Bandwidth = 0.1 to 100 Hz; Background Cell Impedance = 77×10^6 Ω

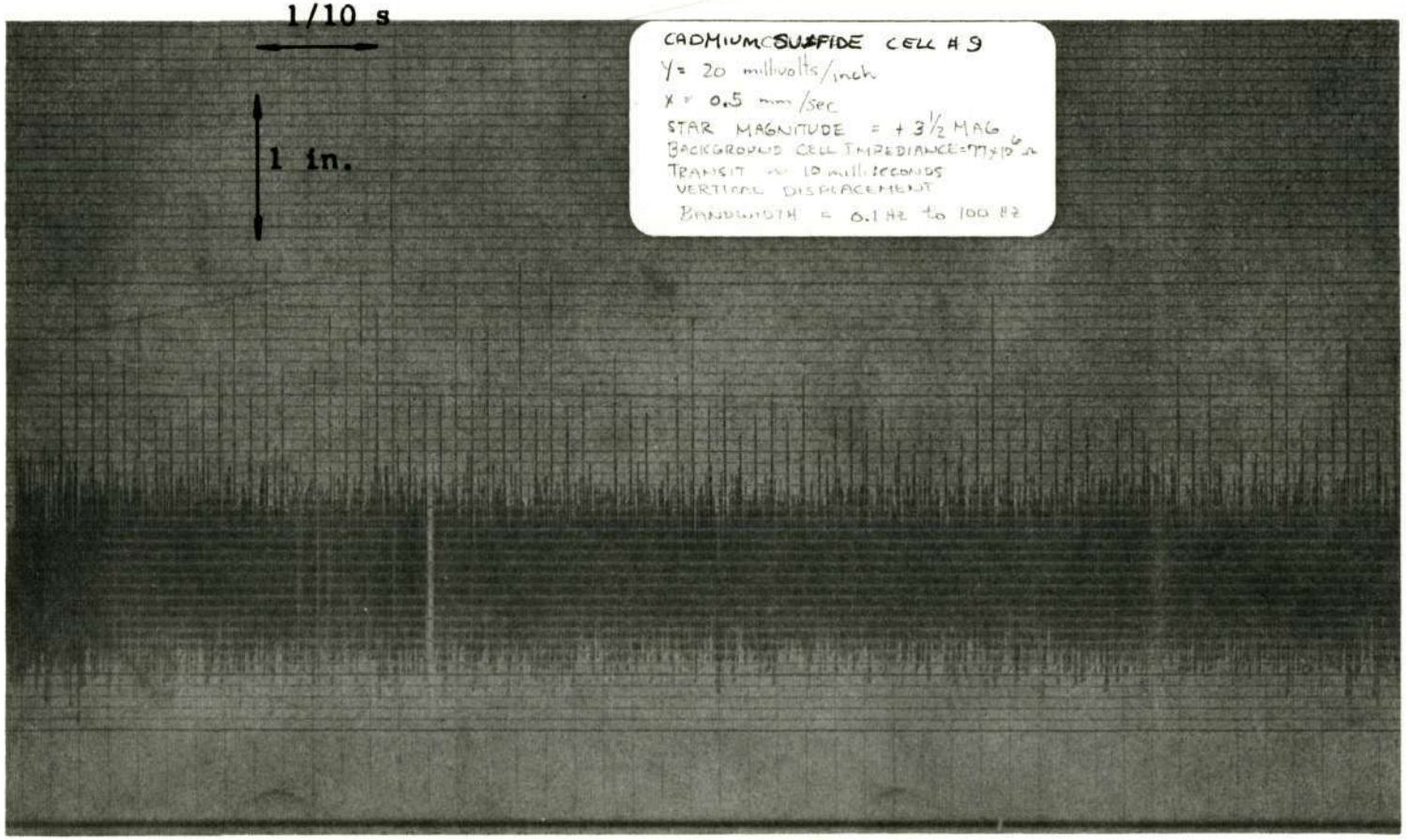

Figure 4.6 CADMIUM SULFIDE CELL NO. 9, y = 20 millivolts/in.; x = 0.5 mm/s; Star Magnitude = + 2.75 Mag; Background Cell Impedance = 77 x 10^6 Ω; Transit ~10 milliseconds; Vertical Displacement; Bandwidth = 0.1 Hz to 100 Hz

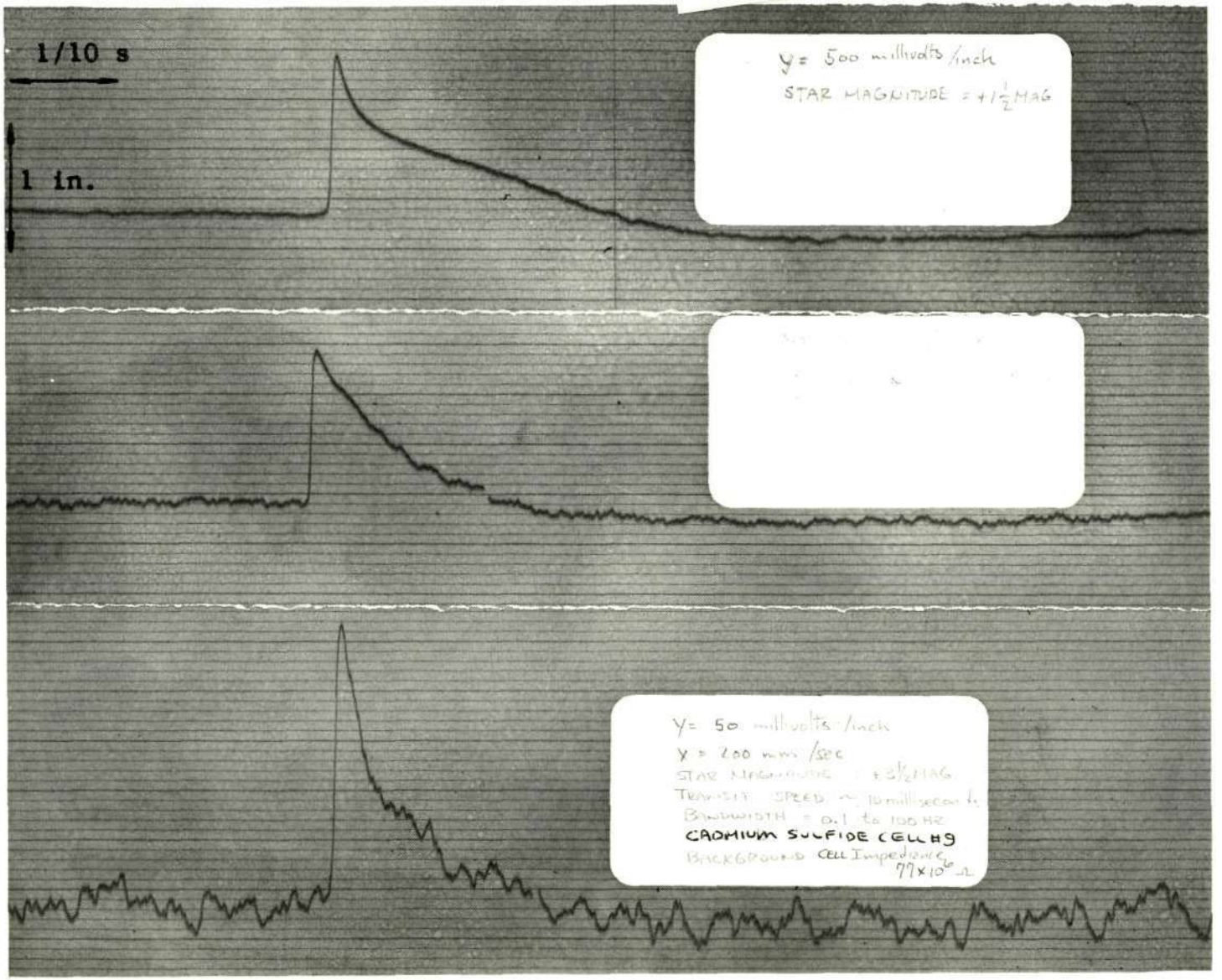

Figure 4.7 CADMIUM SULFIDE CELL NO. 9

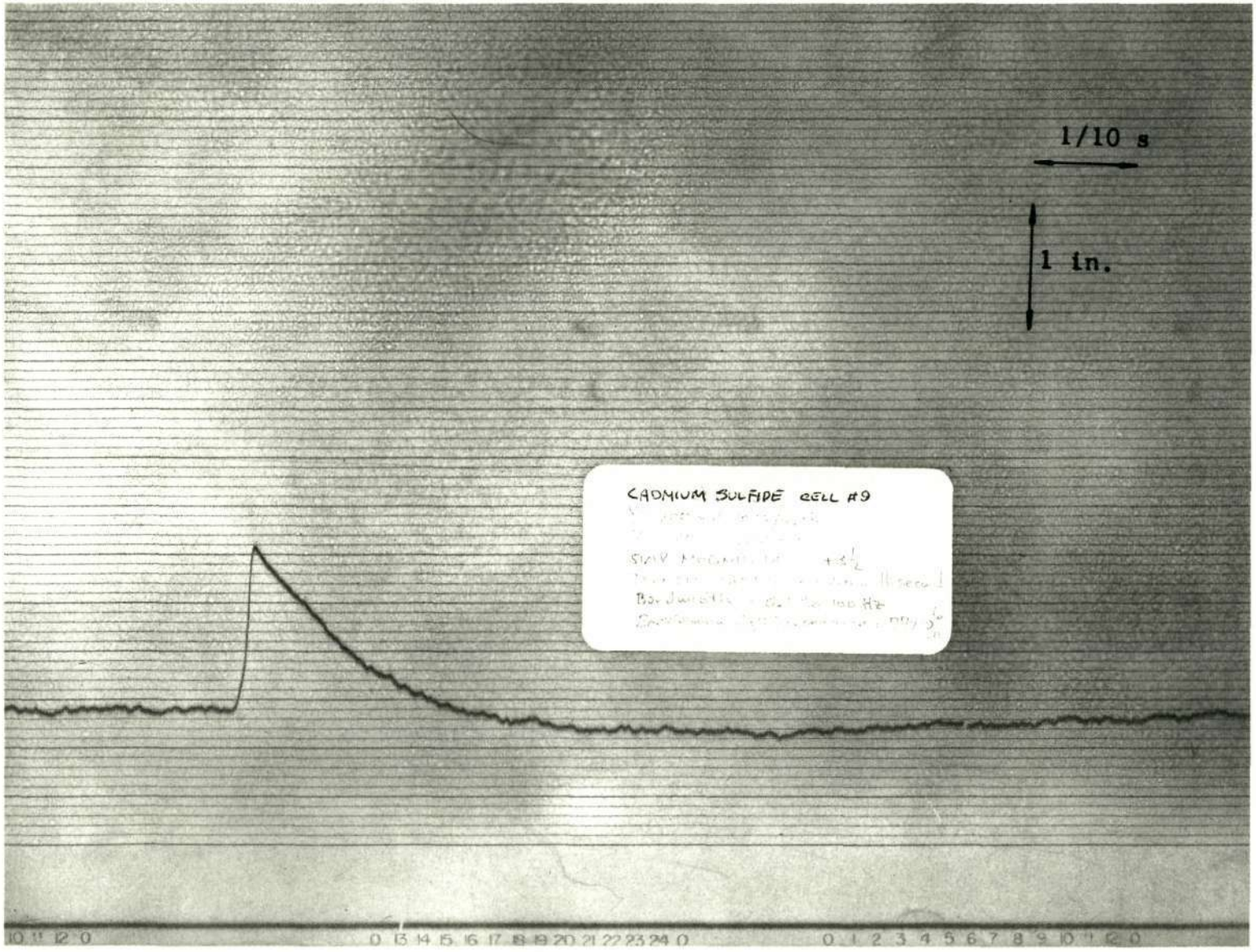

Figure 4.8 CADMIUM SULFIDE CELL NO. 9; y = 200 millivolts/in.; x = 200 mm/s; Star Magnitude = +2.75 ; Transit Speed ~50 millisecond; Bandwidth = 0.1 to 100 Hz; Background Cell Impedance = 77 x 10^6 Ω

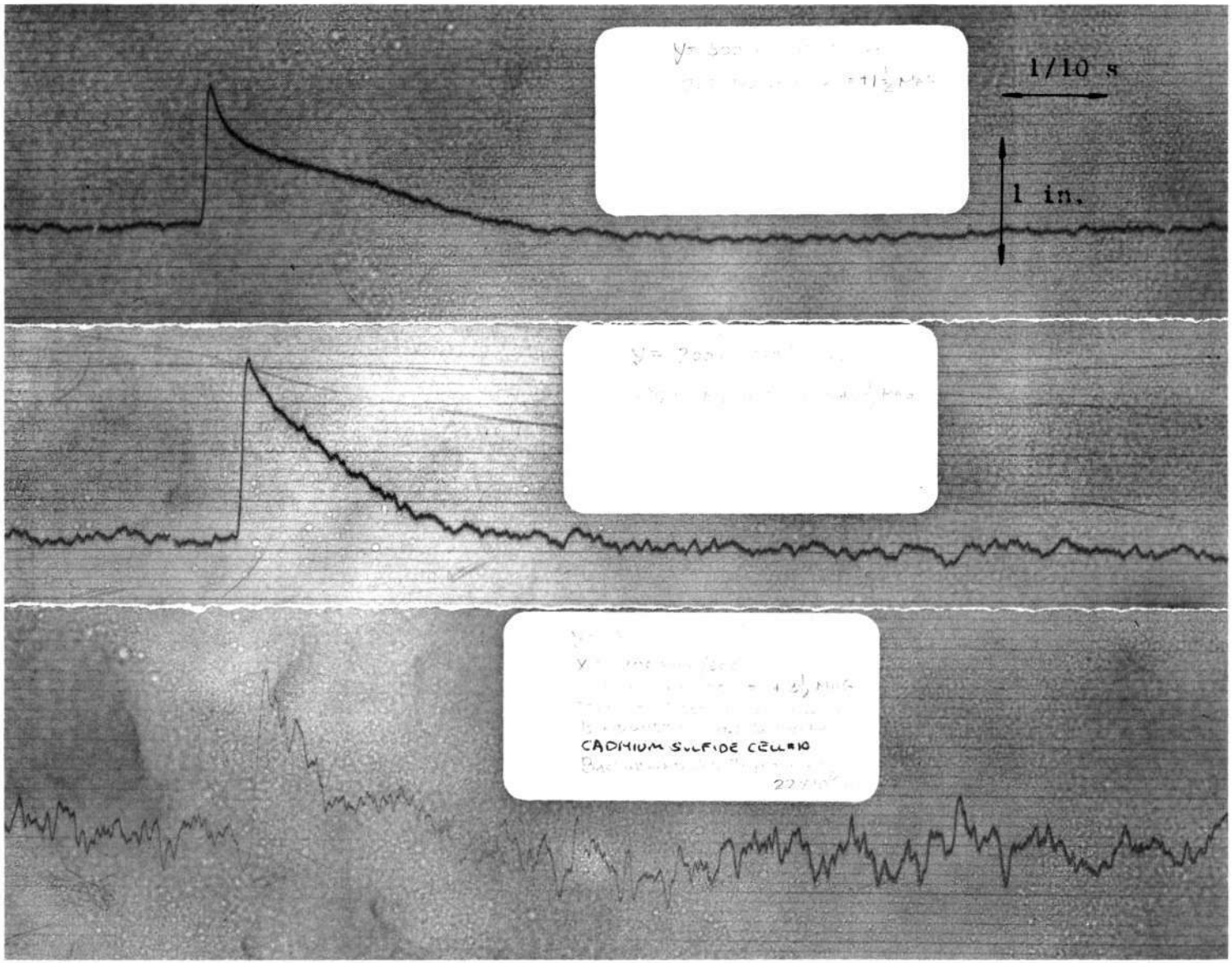

Figure 4.9 CADMIUM SULFIDE CELL NO. 10

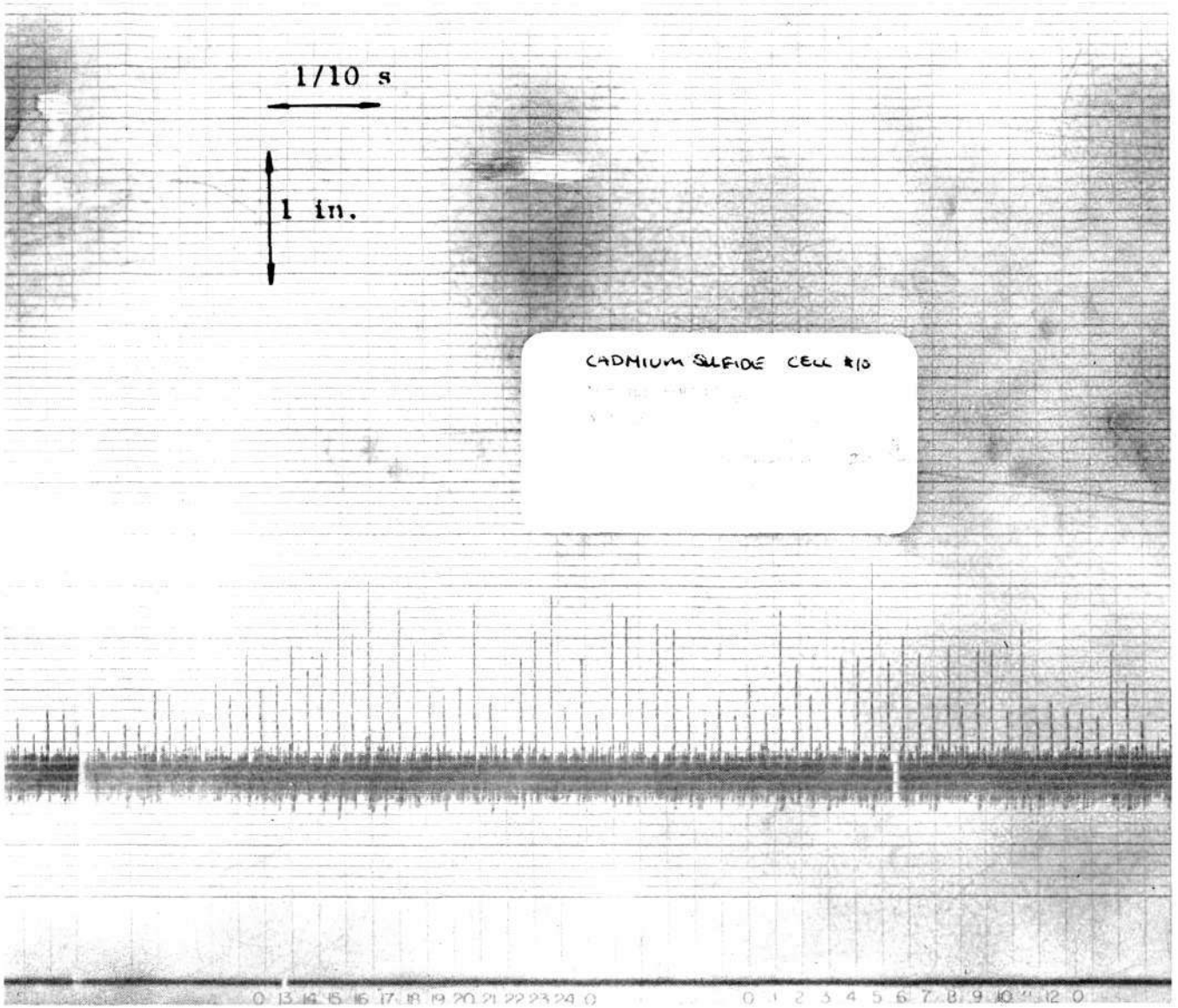

Figure 4.10 CADMIUM SULFIDE CELL NO. 10; y = 100 millivolt/in.; x = 0.5 mm/s; Star Magnitude = +2.25 ; Background Cell Impedance = 22 x 10^6 Ω; Transit ~10 milliseconds; Vertical Displacement; Bandwidth = 0.1 to 100 Hz

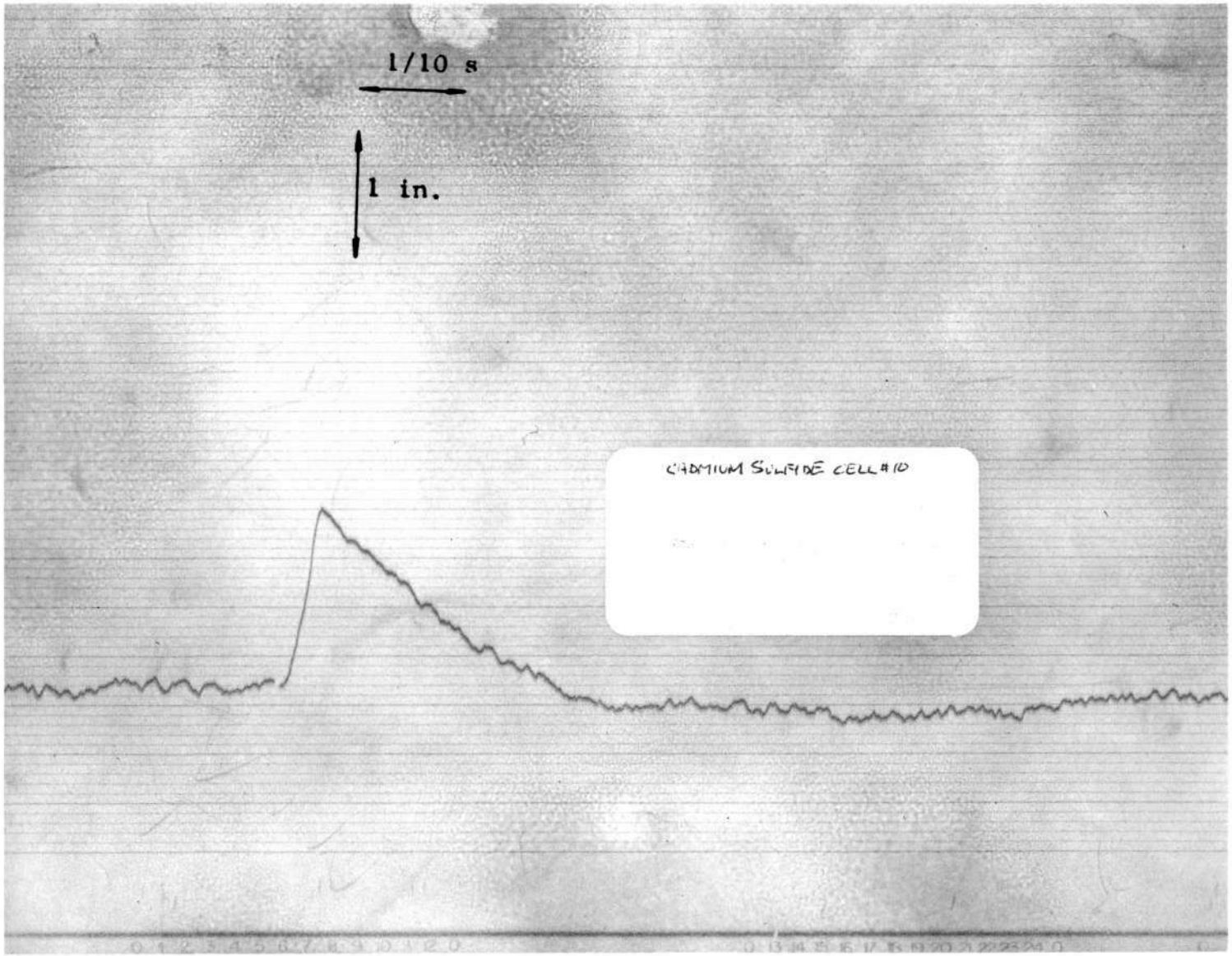

Figure 4.11 CADMIUM SULFIDE CELL NO. 10; y = 200 millivolts/in.; x = 200 mm/s; Star Magnitude = +2.75 Mag; Transit Speed ~50 millisecond; Bandwidth = 0.1 to 100 Hz; Background Cell Impedance = 22 x 10^6 Ω

Cell No.	S/N
8	$\frac{6 \times 1.3}{0.16} = 48.6$
9	$\frac{6 \times 2.25}{0.55} = 24.6$
10	$\frac{6 \times 1.4}{0.70} = 12.0$

Average S/N for 10-millisecond transits = 28

From Figures 4.5, 4.8 and 4.11, the signal/rms noise for 50-millisecond transit rates are:

Cell No.	S/N
8	$\frac{6 \times 1.1}{0.05} = 132$
9	$\frac{6 \times 1.3}{0.12} = 66$
10	$\frac{6 \times 1.4}{0.2} = 42$

Average S/N 50-millisecond transits = 78

The signal/rms noise for both transit rates are shown in Figure 4.12.

4.2.3 Star Transit Pulse Shape

Figures 4.4, 4.5, 4.7, 4.8, 4.10 and 4.11 indicate star transit pulse shape.

Interestingly, bright stars appear to possess a double decay phenomenon associated with the pulse shape. This is created in the amplifier by the protective circuitry in the form of back-to-back diodes that are located in the feedback circuit of the operational amplifier. These diodes prevent amplifier saturation

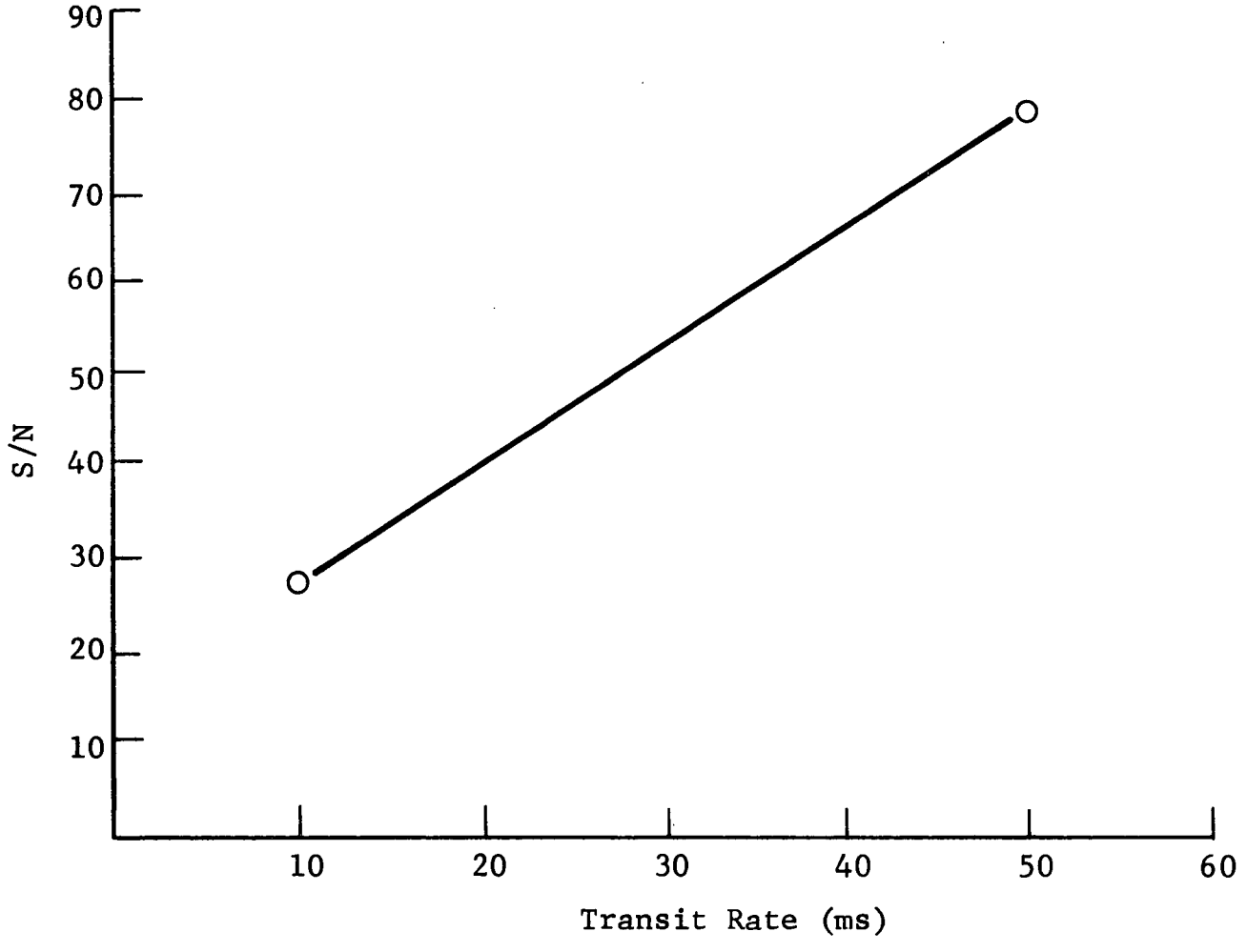

Figure 4.2 STAR SIGNAL/rms NOISE IN TRANSIT RATE

and consequent loss of a sharp peak output results when stars near zero magnitude are transited. The actual peak point in the signal trace is essentially unaffected. This protection is only necessary with cadmium sulfide due to the inherent built-in gain associated with the cadmium sulfide detectors.

4.2.4 Rise Time

Rise times at 2.75-Mag, 1.75-Mag and 0.75-Mag A0 class stars is as follows with 10-millisecond transit times:

Cell No.	Rise Time +2.75 Mag	+1.75 Mag	+0.75 Mag
8	15 ms	12.5 ms	10 ms
9	15 ms	12.5 ms	10 ms
10	16 ms	11 ms	10 ms

The average value of and the maximum deviation from the average rise time of all cells and all star magnitudes is 12.5 milliseconds ± 2.5 milliseconds.

The ±2.5 milliseconds of deviation likely occurs from the voltage scale changes on the recorder. These scale changes preserve the characteristic waveform from the detector. Thus with background illumination there appears to be no trap-filling time in the detector which would create a shortening of the rise time on weak star magnitudes.

4.2.5 Slit Measurements

The cadmium sulfide detector slits were examined under a Unitron TMD-1714 microscope with a 10-power objective. The following slit widths were measured on both ends and the middle of the slit.

Cell No.	Slit Width in Mils End-Center-End		
8	0.4	0.4	0.4
9	0.4	0.4	0.4
10	0.5	0.5	0.5

Slit width is very accurately defined, and no slit deviation from a straight line was observable.

SECTION 5

SILICON FINAL TEST

5.1 DETECTOR TEST DESCRIPTION

The tests described herein were performed to verify the detail requirements for acceptance of silicon slit detectors operating in the short circuit mode.

The test data described herein was recorded on the appropriate data sheets and test results accompany each assembly.

The order of performance of the inspections and tests described herein, was deemed unimportant.

The tests were conducted under the standard room ambient conditions:

a) Temperature; 75 ±10 °F

b) Relative Humidity; less than 75%

5.2 TEST EQUIPMENT

Monochromator, Jarrell Ash model MD 82-000
Chopper,
Light Source Assembly,
Filter,
Dual Axis Stage,
Detector Preamplifier,
Oscilloscope, Tektronix 547 or equivalent
Oscilloscope Plug-in Amplifier, Tektronix Type D
Oscilloscope Plug-in Amplifier, Tektronix Type 1A7A
Function Generator, H/P model 3310A
Filter, Krohn-Hite model 330M
Transistor Curve Tracer, Tektronix model 576
Lite Mike, EG&G model 561
True R.M.S. Electronic Voltmeter, Ballantine Model 320

5.3 DETECTOR TESTS

The tests below determined the following detector parameters.

5.3.1 True Photosensitive Detector Area

5.3.1.1 The equipment was interconnected in accordance with Figure 5.1.

5.3.1.2 The pinhole image size at the detector plane was adjusted to insure it is smaller than the detector slit width from 0.40 μm - 0.99 μm wavelength.

5.3.1.3 The monochromator was set at the wavelengths for which the responsivity will be measured in Section 5.3.5 (i.e. every 500A ° from 4000A° to 9900A°).

5.3.1.4 The 50% and 80% amplitude was measured and recorded while translating the slit both across the detector narrow dimension and also along the long dimension of the detector. See Appendix "C".

5.3.2 Detector Impedance

5.3.2.2 The equipment was interconnected in accordance with Figure 5.2.

5.3.2.2 The detector was placed into a light-tight housing.

5.3.2.3 The function generator output and oscilloscope was adjusted as shown in Figure 5.2.

5.3.2.4 The frequency where the oscilloscope output voltage no longer decreased when the frequency was lowered was determined as point "A" of the representative curve of voltage vs frequency as shown in Figure 5.3.

5.3.2.5 At 0.1 of the frequency "A" determined in 5.3.2.4 the oscilloscope voltage was recorded.

5.3.2.6 The detector resistance was calculated as indicated in appendix A and recorded on the data sheet.

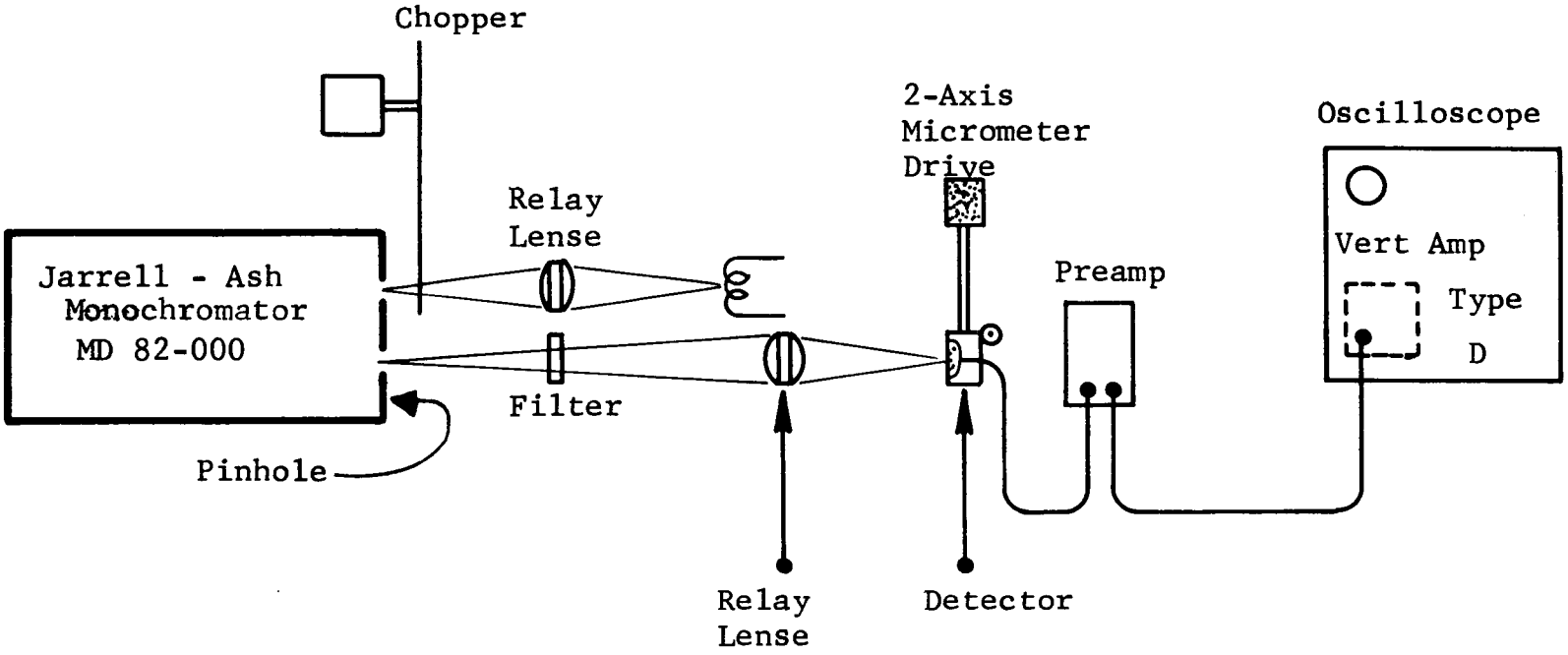

Figure 5.1 INTERCONNECTION DIAGRAM FOR MONITORING DETECTOR AREA

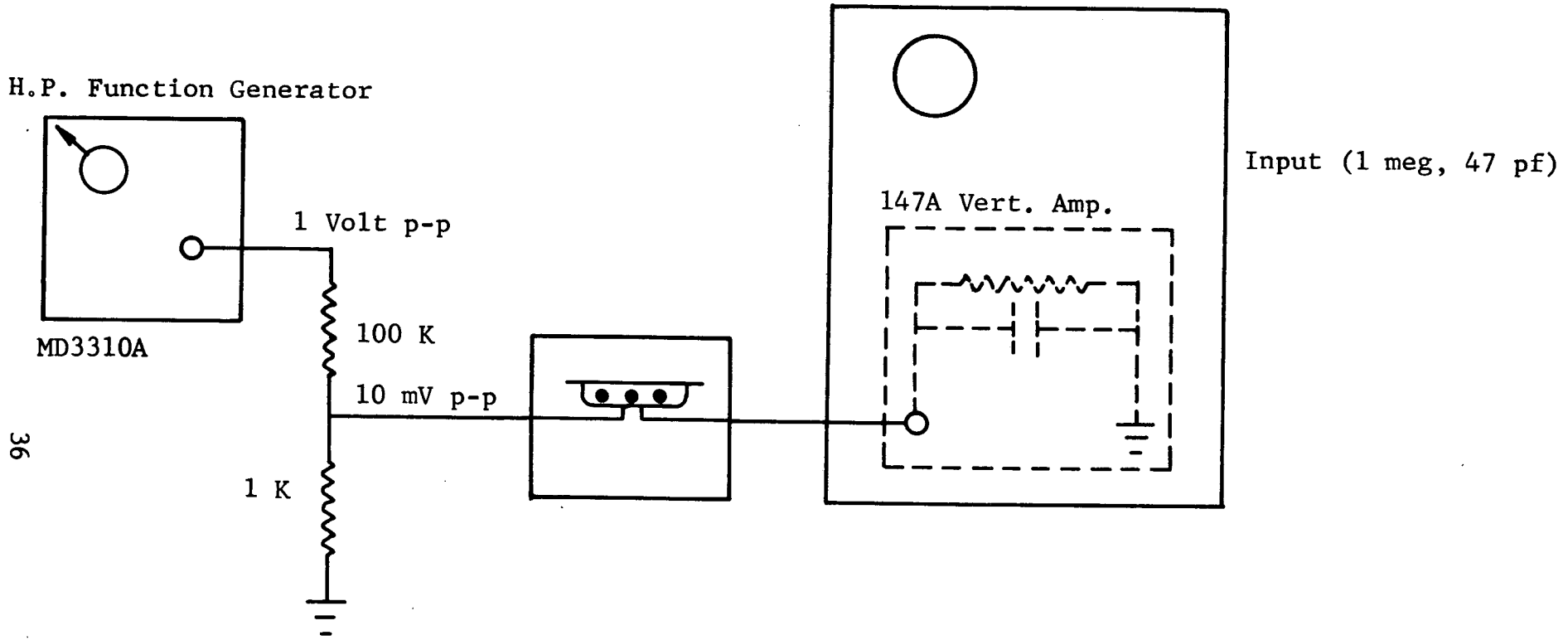

Figure 5.2 INTERCONNECTION DIAGRAM FOR MONITORING DETECTOR IMPEDANCE

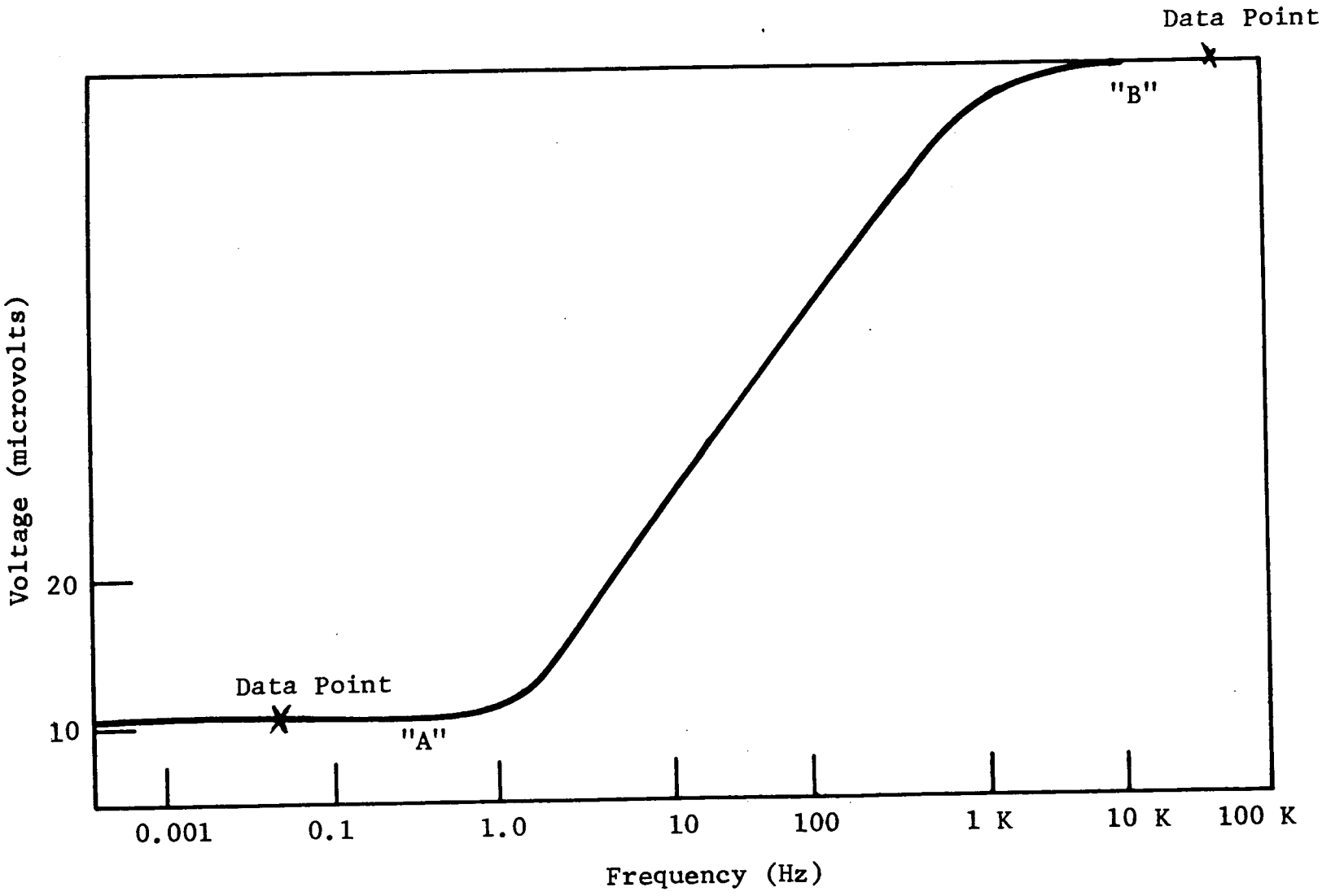

Figure 5.3 LOCATION OF DATA POINTS FOR MONITORING DETECTOR IMPEDANCE

5.3.2.7 The frequency, where the oscilloscope output voltage no longer increases if the frequency is raised, was determined as point "B" of the representative curve of voltage vs frequency as shown in Figure 5.3.

5.3.2.8 At 10 times the frequency "B" determined in 5.3.2.7, the oscilloscope voltage was recorded.

5.3.2.9 The detector capacitance was calculated as indicated in appendix A and recorded on the data sheet.

5.3.3 Noise Current

5.3.3.1 The equipment was interconnected in accordance with Figure 5.4.

5.3.3.2 The gain of the system was calibrated for the following bandpasses:

0.2 - .315 Hz
0.315 - 1.0 Hz
1.0 - 3.15 Hz
3.15 - 10 Hz
10 - 31.5 Hz
31.5 - 100 Hz
100 - 315 Hz
315 - 1000 Hz - - - by the following technique.

A. 1A7A and Khron-Hite Gain

The output lead of detector preamplifier was disconnected.

This lead, the input lead of the 1A7A vertical amplifier, was then connected to the function generator of Figure 5.2.

With the Khron-Hite filter set for one of the bandpasses listed above, the function generator was swept and the 3 dB voltage frequencies were recorded; 2nd, the function generator was set at midband and the voltage gain for all useable settings of 1A7A vertical preamplifier were recorded.

This procedure was repeated with the Khron-Hite filter set for each of the bandpasses listed above.

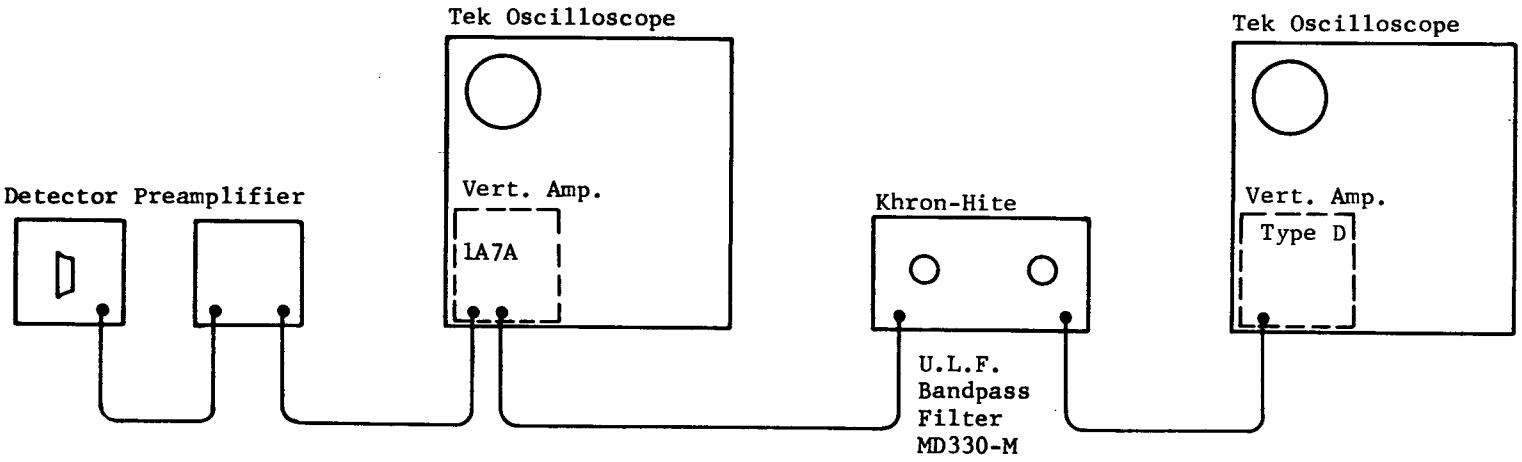

Figure 5.4 INTERCONNECTION DIAGRAM FOR MONITORING NOISE CURRENTS

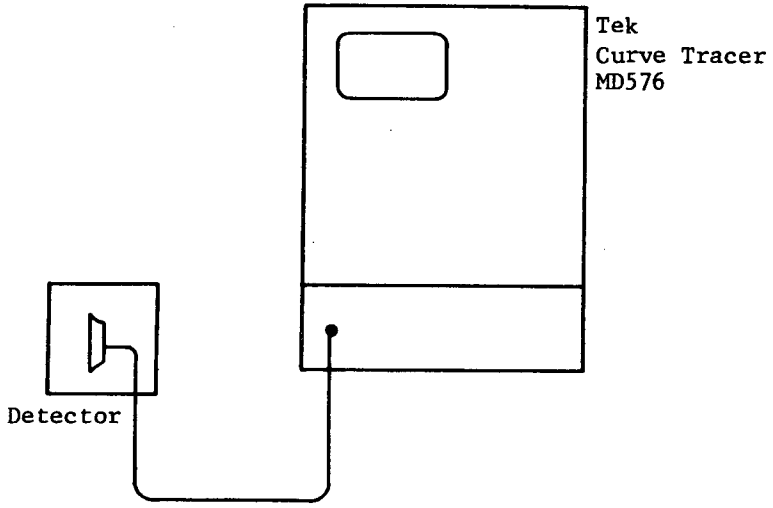

Figure 5.5 INTERCONNECTION DIAGRAM FOR MONITORING DARK CURRENT

Upon completion of the calibration of the 1A7A and the Khron-Hite filter, the function generator was disconnected and the detector/preamplifier lead reconnected.

B. Preamplifier Gain

The detector was then removed and replaced with a series precision resistor and a shunt capacitor equal to the lowest measured R and highest measured C values of the detectors measured in Section 5.3.2. The resistor was connected to the function generator and resistor divider network of Figure 5.2. The function generator was swept over the same bandpass listed above, and the voltage gain recorded. The voltage gain was converted to current-to-voltage gain and recorded. Following the preamplifier Gain Calibration, the input precision resistor and capacitor were disconnected. Consecutively, the following items were reconnected to the preamplifier input terminals.

DETECTOR #1
CAPACITOR equal to Detector #1 Capacity

DETECTOR #2
CAPACITOR equal to Detector #2 Capacity

DETECTOR #3
CAPACITOR equal to Detector #3 Capacity

5.3.3.3 The output voltage in the above passbands of 5.3.3.2 was recorded.

5.3.3.4 The noise current per root cycle from the data in 5.3.3.2 and 5.3.3.3 was calculated as indicated in Appendix B. The results are plotted on the data sheets.

5.3.4 Dark Current

5.3.4.1 The equipment was interconnected as shown in Figure 5.5 with the detector located in a light-tight housing.

5.3.4.2 The voltage where the reverse current reached 1 μA was measured and recorded on the data sheet.

5.3.4.3 At a voltage equal to 0.5 of the voltage determined in 5.3.4.2, the current was measured and recorded on the data sheet.

5.3.5 Absolute Spectral Response

5.3.5.1 The equipment was interconnected as shown in Figure 5.6.

5.3.5.2 The slit image at the test plan was measured and verified to be less in length and width than the Lite-Mike detector dimensions.

5.3.5.3 The Lite-Mike was inserted at the test plane and aligned to collect all the energy.

5.3.5.4 The absolute energy was measured and recorded at the test plane every 500 Å from 4000 Å to 9900 Å.

5.3.5.5 The Irradiance was calculated at the detector test plane for the data points of 5.3.5.4.

5.3.5.6 The Lite-Mike was removed and the detector inserted at the test plane as shown in Figure 5.7.

5.3.5.7 The pinhole was inserted as shown in Figure 5.7 and the pinhole image was measured at the test plane to verify that the image is smaller in diameter than the slit width at all wavelength as indicated in appendix "C".

5.3.5.8 The pinhole image was aligned to collect all the energy. The voltage output from preamplifier was recorded at the wavelengths of step 5.3.5.4.

5.3.5.9 The data was recorded and the average responsivity of the entire detector slit calculated as indicated in Appendix "D". The results were plotted on the data sheets.

5.3.6 Uniformity

5.3.6.1 The equipment was again interconnected as shown in Figure 5.7.

5.3.6.2 The same pinhole used in Section 5.3.5.7 was inserted.

5.3.6.3 The monochromator was located at 5500Å.

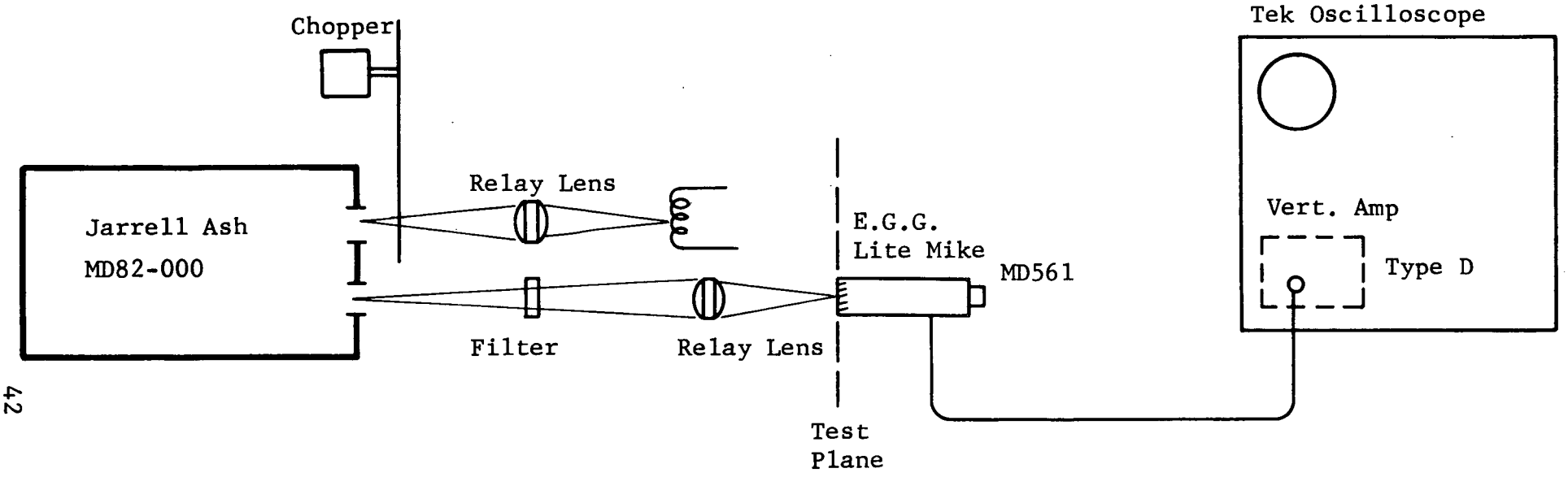

Figure 5.6 INTERCONNECTION DIAGRAM FOR CALIBRATION OF THE ABSOLUTE SPECTRAL RESPONSE

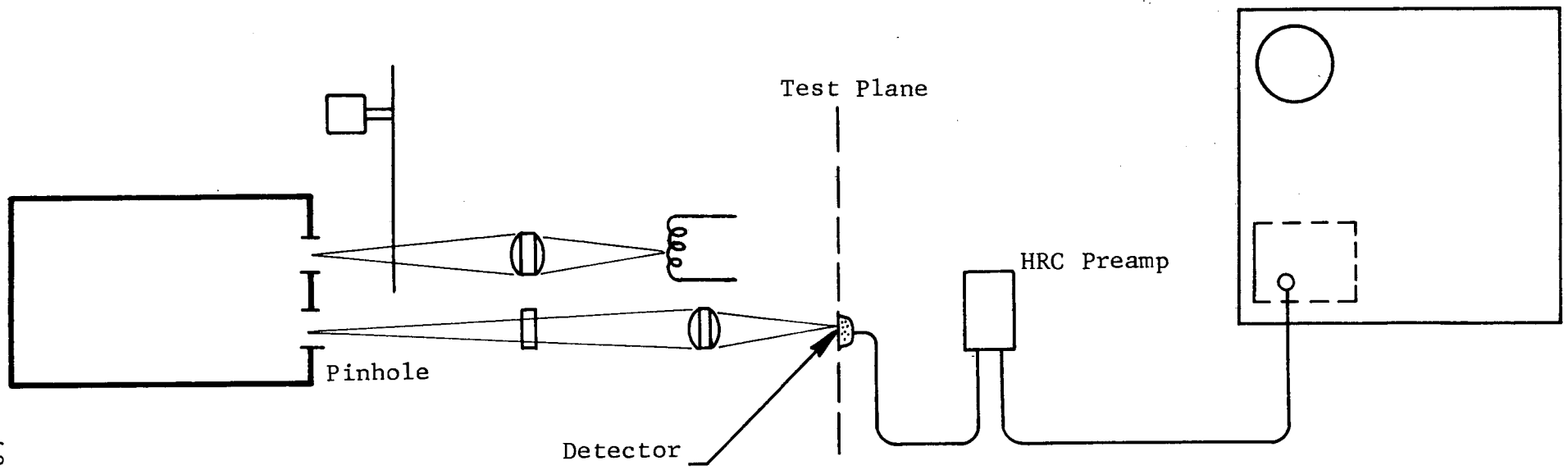

Figure 5.7 INTERCONNECTION DIAGRAM FOR MONITORING THE DETECTOR ABSOLUTE SPECTRAL RESPONSE

5.3.6.4 The pinhole image was centered on the detector every 25 mils along the 500 mil detector length.

5.3.6.5 The output voltage was recorded every 25 mils along the detector.

5.3.6.6 The average responsivity was calculated at 5500 A°.

5.3.6.7 The responsivity was plotted along the detector versus detector segment on data sheet.

5.3.7 Noise Equivalent Power

5.3.7.1 The value of the noise current from Section 5.3.3.4 was tabulated on the high frequency basin of the plot of noise current versus frequency. On this basin, the voltage noise contribution of the preamplifier reflected from the detector capacity as a noise current, has been eliminated and all 1/f noise has disappeared.

5.3.7.2 Using the resulting noise current of the detector and the measured value of the maximum responsivity from the responsivity plot, the noise equivalent power was calculated in watts for a 1-Hz bandwidth and recorded on the data sheet.

5.3.8 Detectivity (D*)

5.3.8.1 The value calculated for NEP in Section 5.3.7 was tabulated.

5.3.8.2 The value of the active cell area from the values of the active cell length and width at the frequency of maximum responsivity as measured in Section 5.3.1 was calculated.

5.3.8.3 The detectivity D^*_λ was then calculated in cm $(Hz)^{1/2}$/watt from the values of 5.3.8.1 and 5.3.8.2 and record on the data sheet.

5.3.9 Visual Inspection

5.3.9.1 The detectors underwent microscopic inspection

(10x) for contamination and workmanship according to HRC Detector workmanship standards including surface contamination and defects in the active area.

5.3.9.2 The lead bonding was examined (10x) for proper adherence and protection including adequate service loops.

5.3.9.3 The detectors were inspected for conformance with part drawing.

5.4 Detector Test Results

The following pages contain the complete set of measured detector parameters as obtained by the techniques described in section 5.3. Figures 5.8, 5.9 and 5.10 show absolute spectral responsivity, Figures 5.11, 5.12 and 5.13 show uniformity; and Figures 5.14, 5.15 and 5.16 show detector Noise spectrum.

DATA SHEET

Detector Serial Number 1

Cell Width	2.05 MILS
Cell Length	510 MILS
Cell Resistance	199 MEGOHMS
Cell Capacitance	308 PICOFARADS

Reverse Voltage for 1 μA Current 15.6 VOLTS

Leakage Current at 7.8 Volts 55 NANOAMPS

Noise Equivalent Power

@ 0.67 μm wavelength 6.06×10^{-14} watts

@ 200 Hz center freq.

@ 1 Hz bandwidth

@ <-1.0 mV bias

Detectivity

@ 0.67 μm wavelength 1.36×10^{12} $\frac{\text{cm Hz}^{1/2}}{\text{watts}}$

@ 200 Hz center freq.

@ 1 Hz bandwidth

@ <-1.0 mV bias

Preamplifier used for Test No. DEK 20A1

DATA SHEET

Detector Serial Number 2

Cell Width	2.26	MILS
Cell Length	505	MILS
Cell Resistance	499	MEGOHMS
Cell Capacitance	346	PICOFARADS
Reverse Voltage for 1 μA Current	15.9	VOLTS
Leakage Current at 7.95 Volts	2.8	NANOAMPS

Noise Equivalent Power

@ 0.70 μm	wavelength	2.34×10^{-14}	watts
@ 200 Hz	center freq.		
@ 1 Hz	bandwidth		
@ <-1.0mV	bias		

Detectivity

@ 0.70 μm	wavelength	3.66×10^{12}	$\frac{\text{cm Hz}^{1/2}}{\text{watts}}$
@ 200 Hz	center freq.		
@ 1 Hz	bandwidth		
@ <-1.0mV	bias		

Preamplifier used for Test No. DEK 20A1

DATA SHEET

Detector Serial Number 3

Cell Width	2.06 MILS
Cell Length	495 MILS
Cell Resistance	10.8 MEGOHMS
Cell Capacitance	308 PICOFARADS
Reverse Voltage for 1 μA Current	8.2 VOLTS
Leakage Current at 4.1 Volts	350 NANOAMPS

Noise Equivalent Power

@ 0.77 μm	wavelength	12.3×10^{-14} watts
@ 200 Hz	center freq.	
@ 1 Hz	bandwidth	
@ <-1.0 mV	bias	

Detectivity

@ 0.77 μm	wavelength	0.658×10^{12} $\frac{\text{cm Hz}^{1/2}}{\text{watts}}$
@ 200 Hz	center freq.	
@ 1 Hz	bandwidth	
@ <-1.0 mV	bias	

Preamplifier used for Test No. DEK 20A1

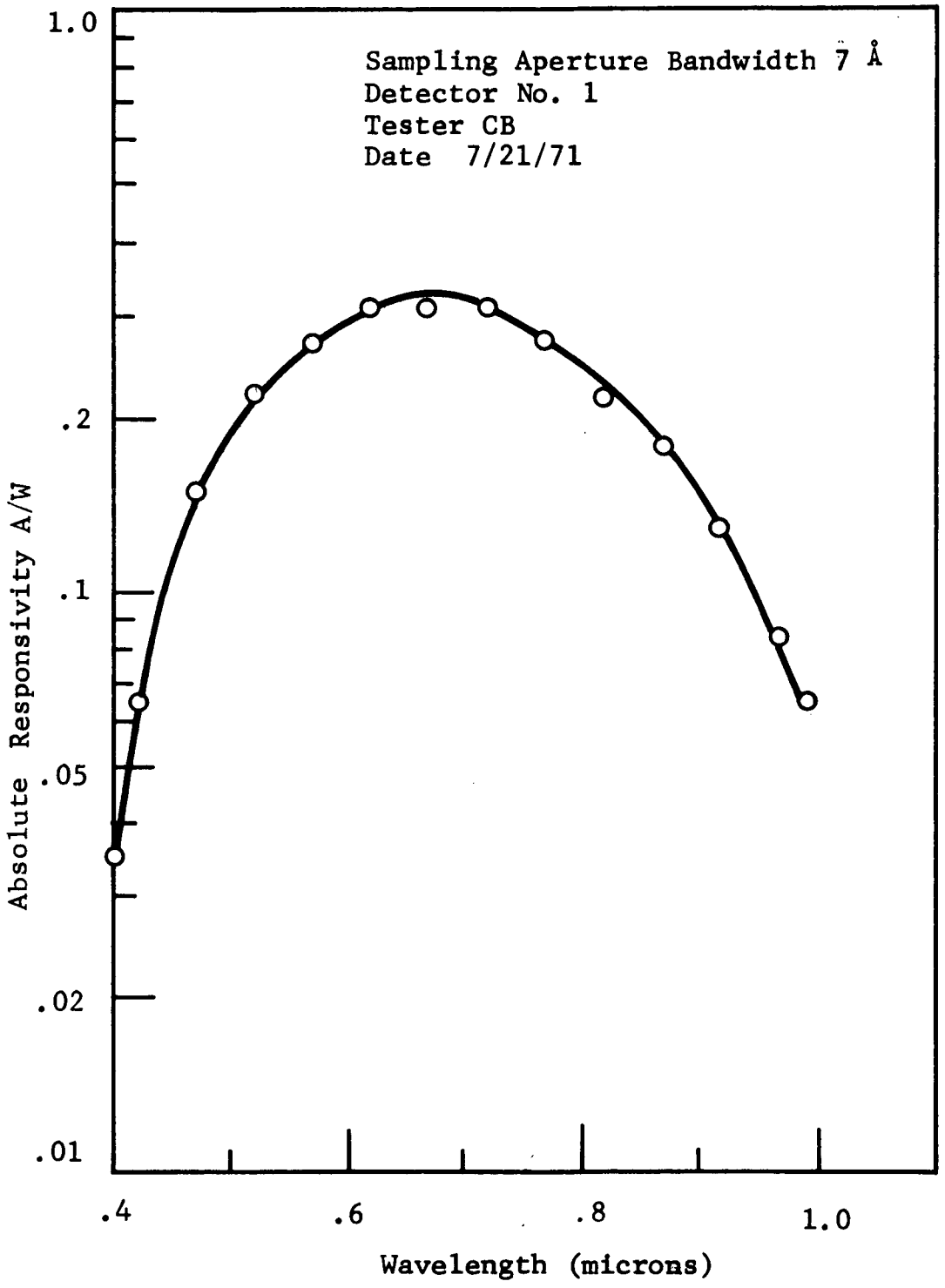

Figure 5.8 ABSOLUTE SPECTRAL RESPONSIVITY

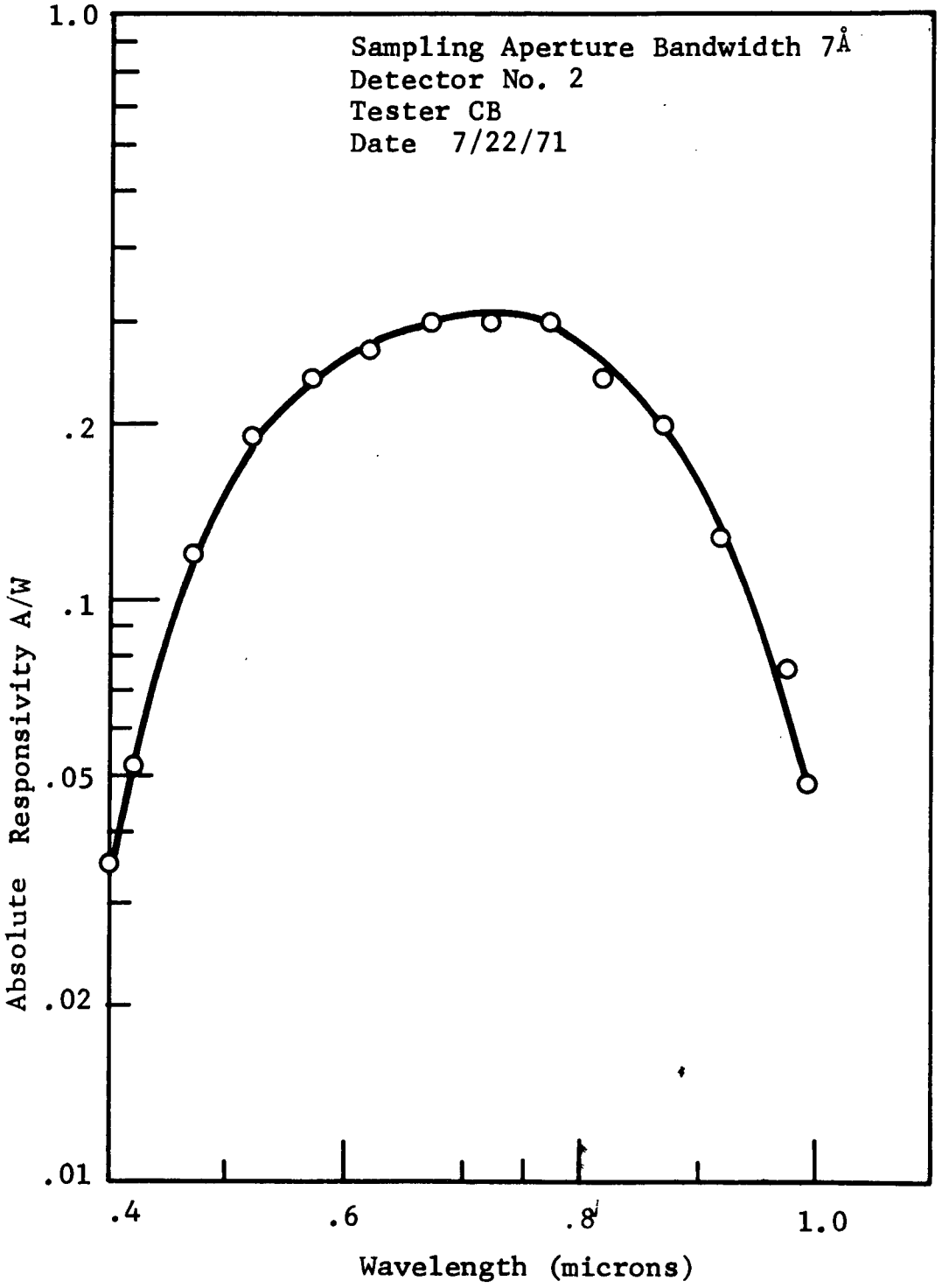

Figure 5.9 ABSOLUTE SPECTRAL RESPONSIVITY

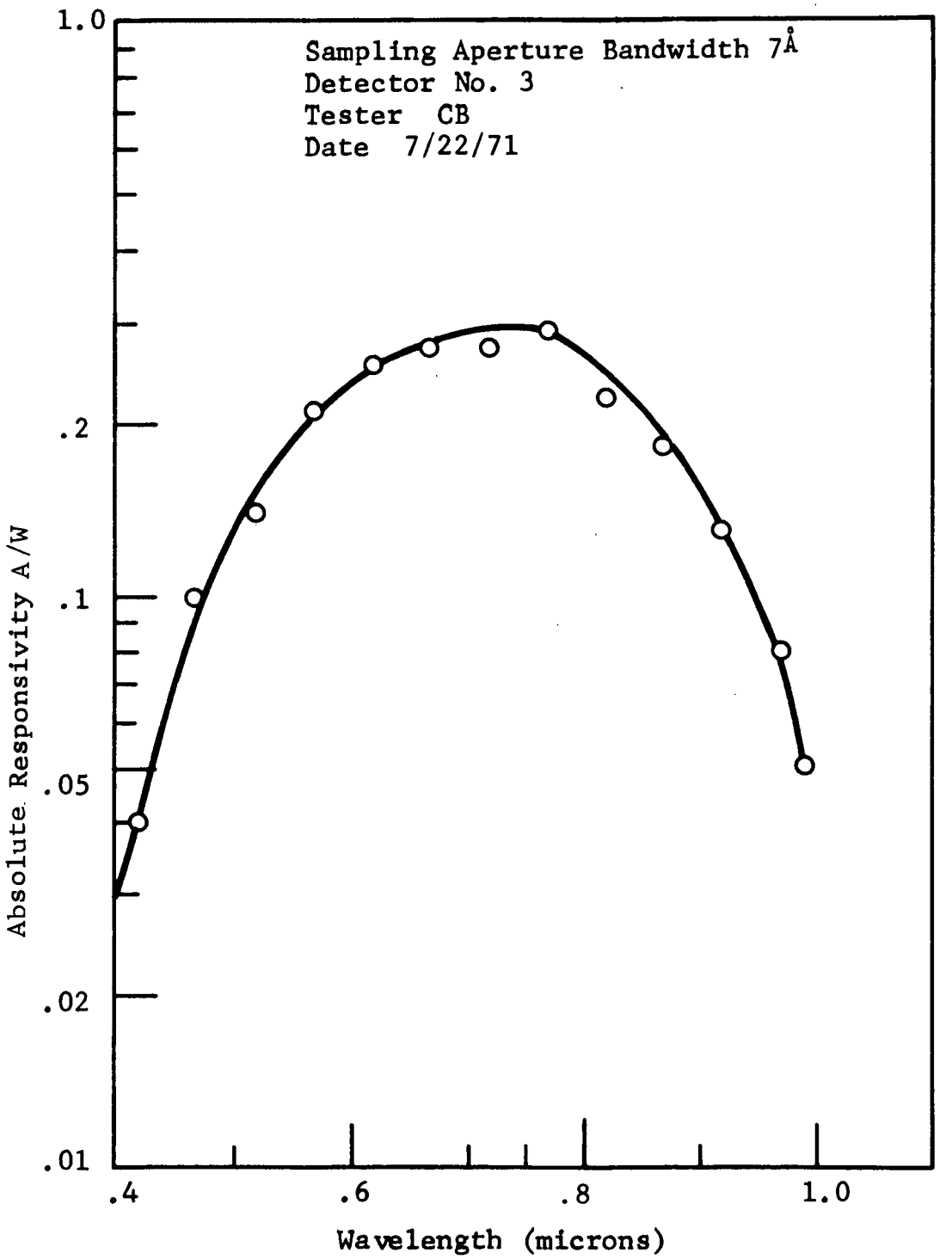

Figure 5.10 ABSOLUTE SPECTRAL RESPONSIVITY

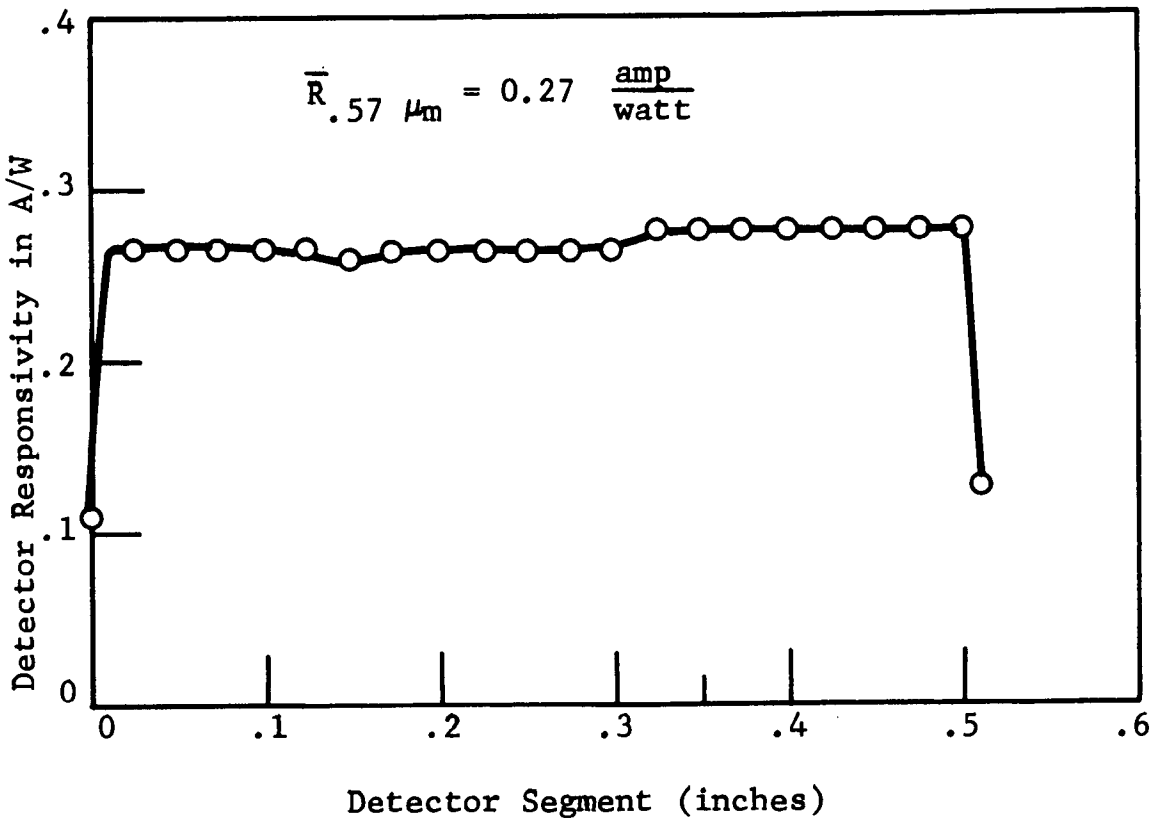

Sampling Aperture Bandwidth 7Å
Sampling Aperture Center Wavelength 0.57 μm
Sampling Aperture Size 1.5 mil dia
Detector No. 1
Tester CB
Date 7/21/71

Figure 5.11 DETECTOR UNIFORMITY

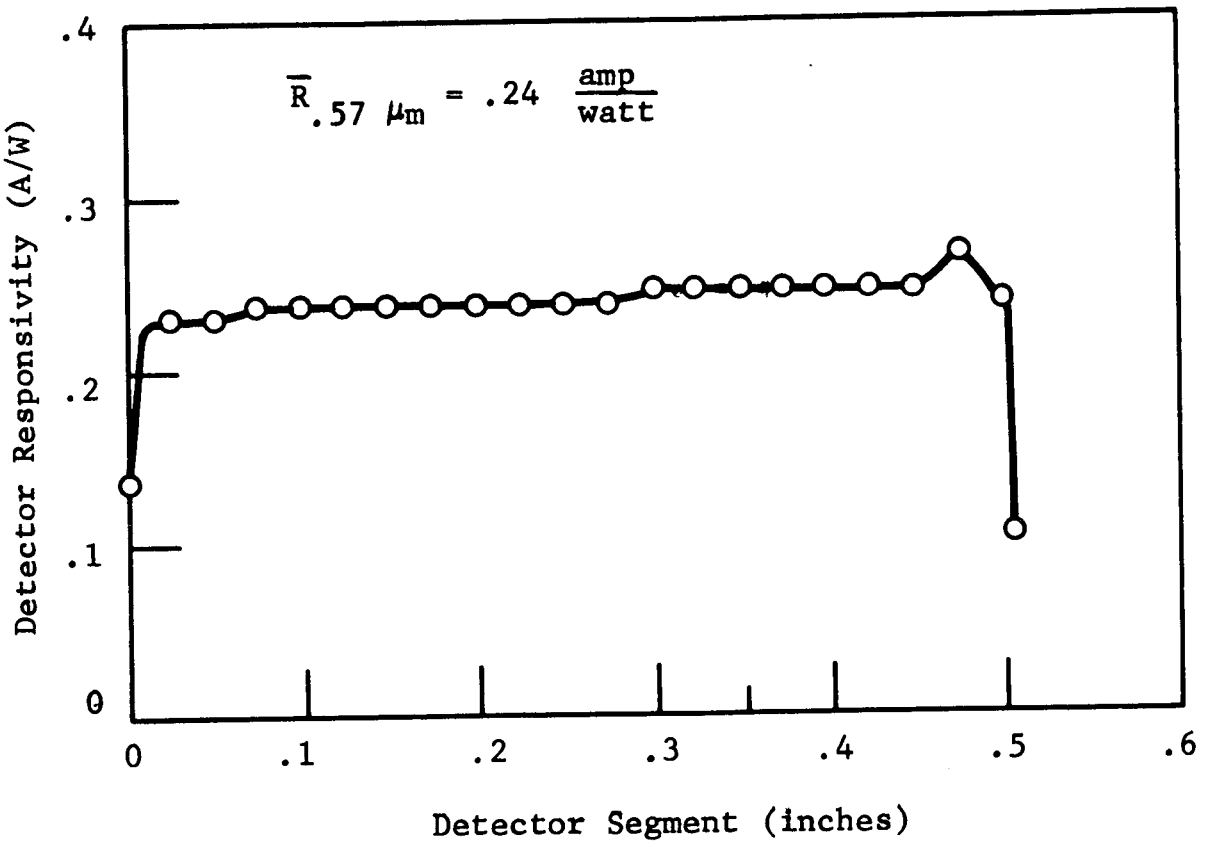

Sampling Aperture Bandwidth 7Å
Sampling Aperture Center Wavelength 0.57 μm
Sampling Aperture Size 1.5 mil dia
Detector No. 2
Tester CB
Date 7/22/71

Figure 5.12 DETECTOR UNIFORMITY

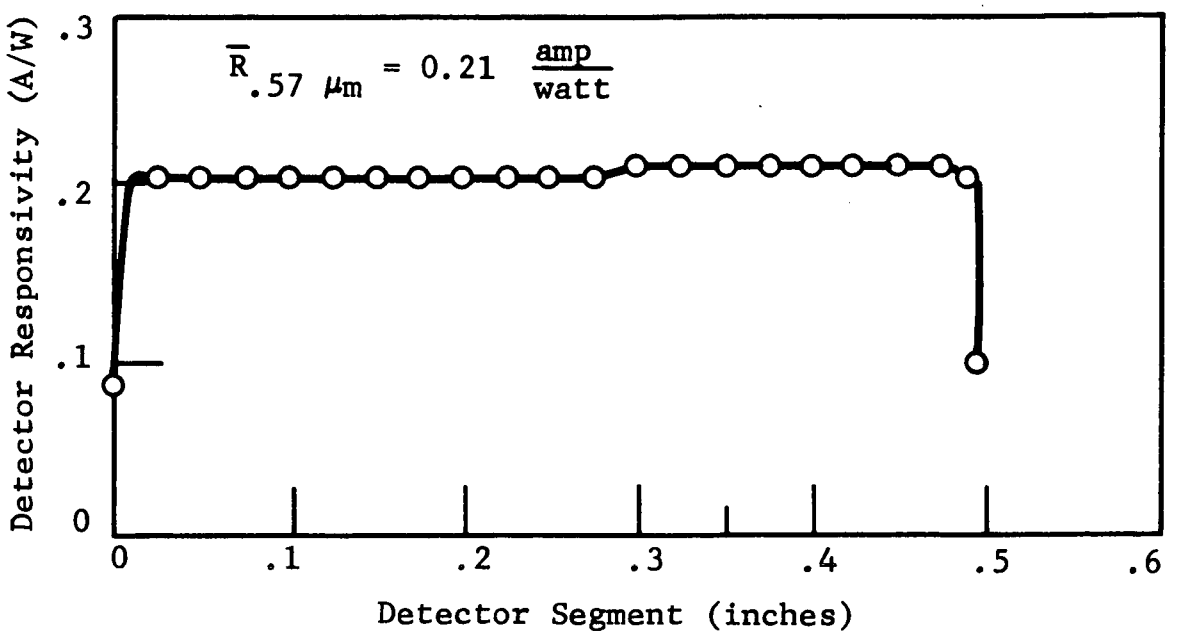

Sampling Aperture Bandwidth 7Å
Sampling Aperture Center Wavelength 0.57 μm
Sampling Aperture Size 1.5 mil dia
Detector No. 3
Tester CB
Date 7/22/71

Figure 5.13 DETECTOR UNIFORMITY

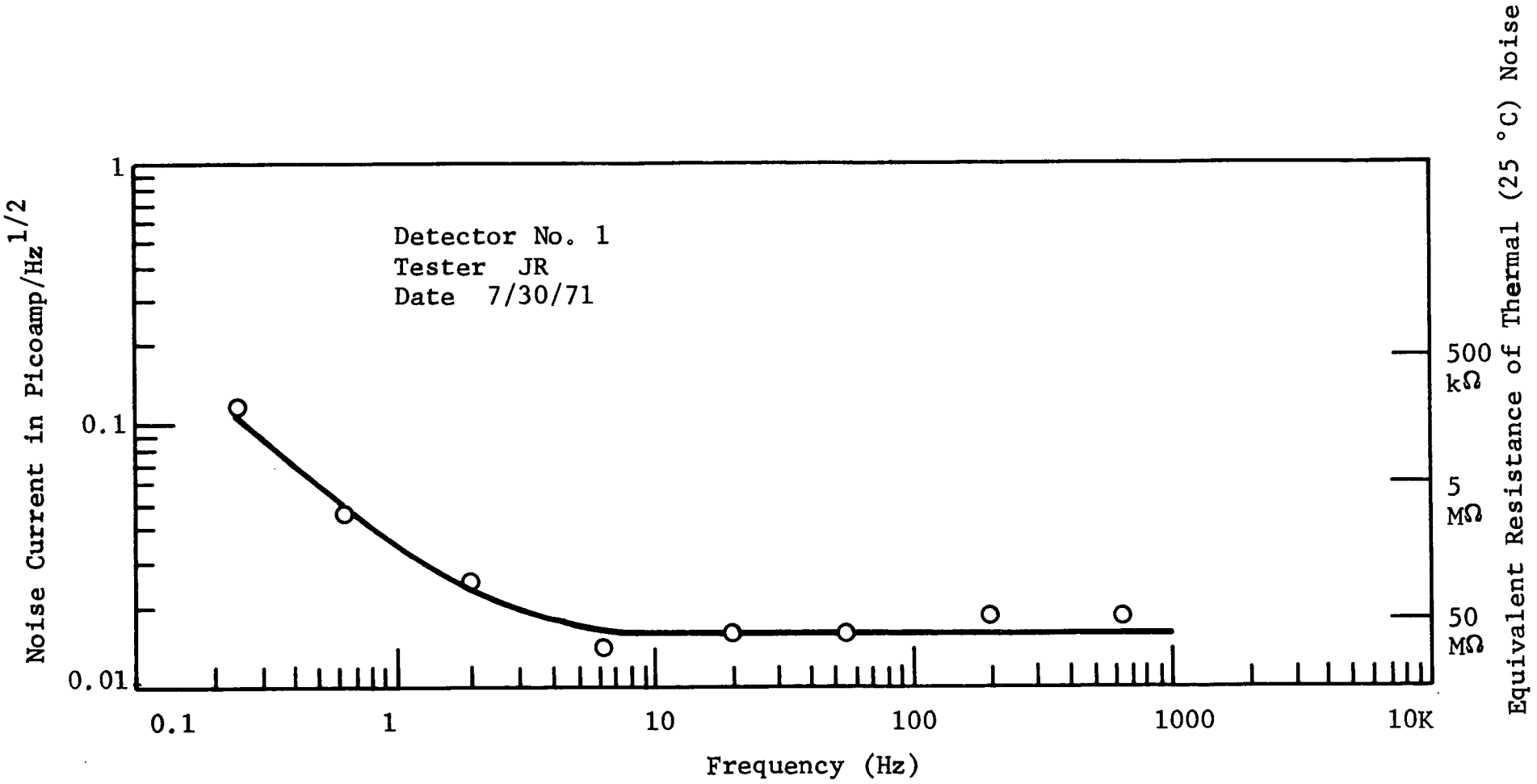

Figure 5.14 SILICON DETECTOR NOISE SPECTRUM

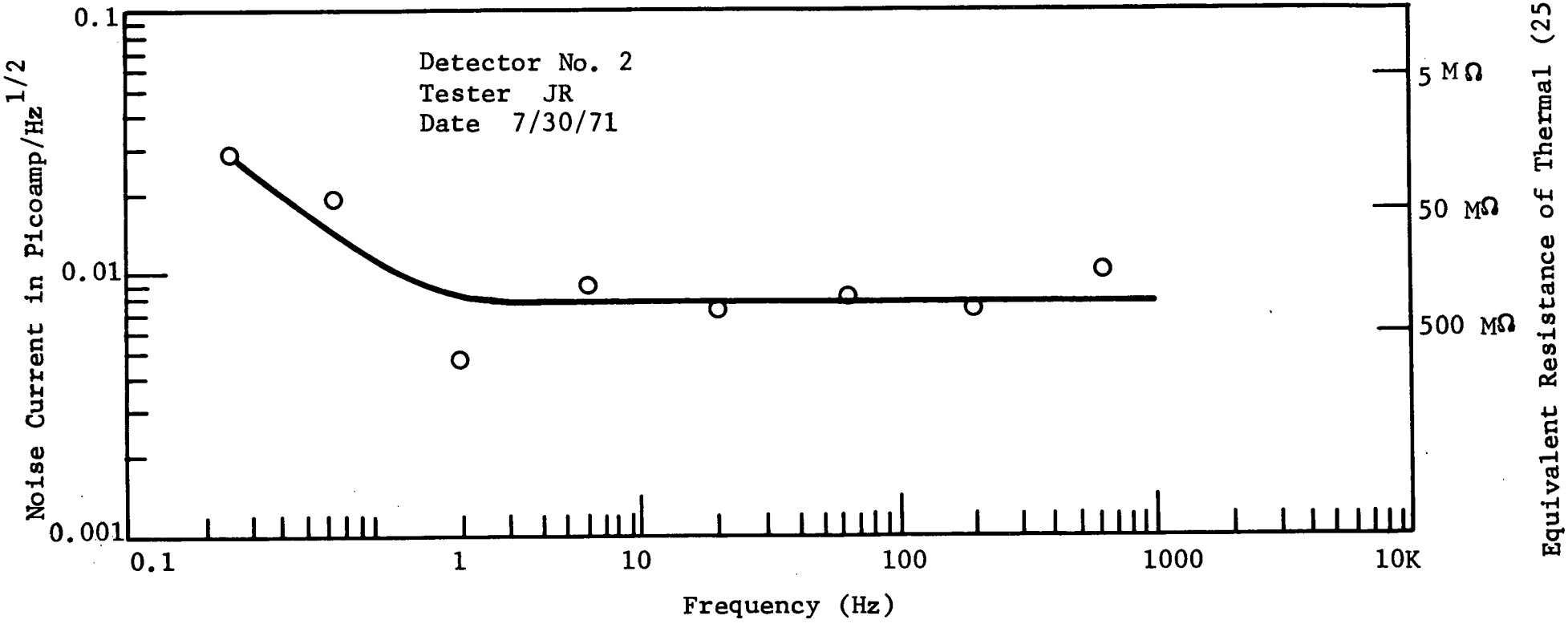

Figure 5.15 SILICON DETECTOR NOISE SPECTRUM

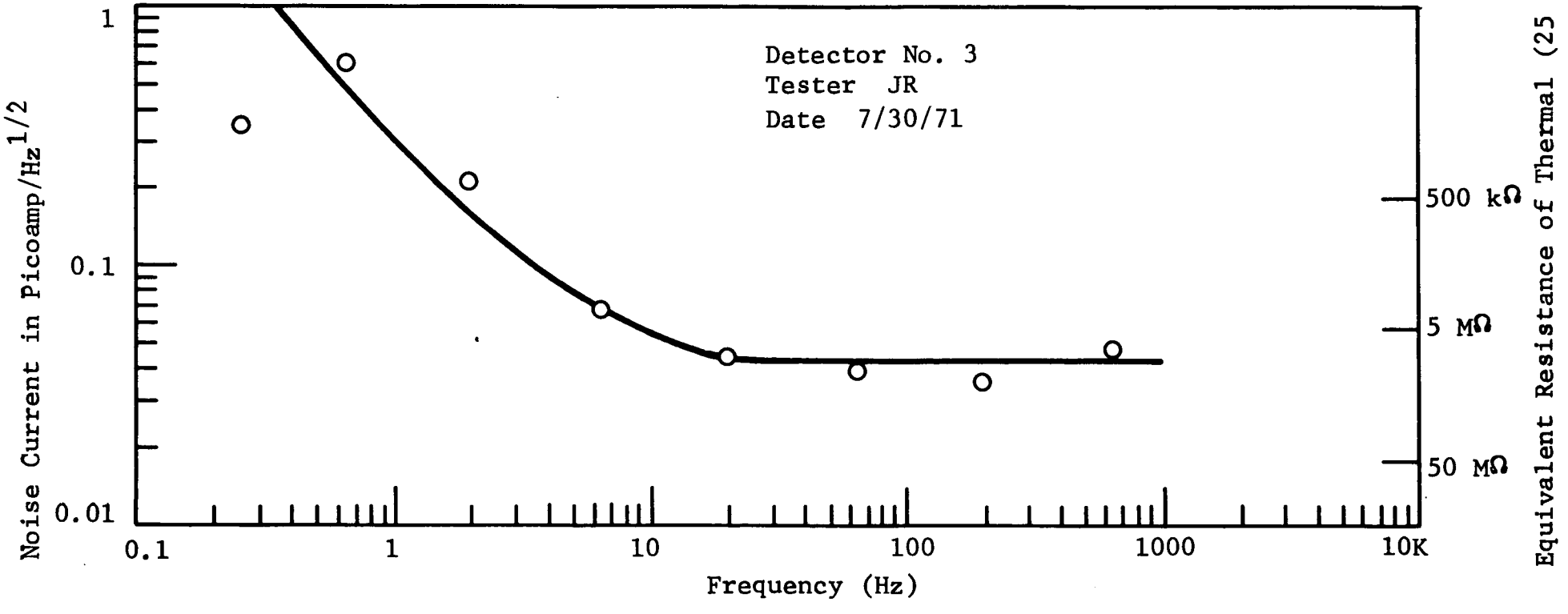

Figure 5.16 SILICON DETECTOR NOISE SPECTRUM

5.5 Theoretical Star Signal

Using the Spectral responsivity results of section 5.4, a calculation was made of the expected level of the detector output when the silicon detector no. 2 is used in the following manner.

A. The detector being located at the focal plane of a 3.0-inch effective diameter optical system.

B. The total overall efficiency of the optical system being described by 80% of the incident energy on the optical system being focused on a region of the photo-sensitive area of the detector.

C. The source of energy being an M-5 class star (2800 °K color temperature) which in section 5.6 will be simulated by an unfiltered 6-V 9-A ribbon filament lamp operating at 8 amperes and removes uncertainties associated with color filtering for establishing different star classes.

D. The glass window covering of the detector being removed to maximize the energy incident on this detector at 80%.

The following calculation was carried out on a computer. The absolute radiometric spectral distribution of a 0.0 magnitude M-5 class star was determined by performing the following calculations:

A. Multiplying the response curve of the human eye with a 2800 °K (M5 star class) spectral distribution.

B. Integrating the result from 0.38 to 0.76 μm

C. Normalizing this result to obtain the constant to make the result of B contain 2.57×10^{-6} lumen/m^2 which is the photometric energy density of any class 0 mag star.

$$K = \frac{2.57 \times 10^{-6} \text{ lumens/m}^2}{\int_{.38\mu}^{.76\mu} BB(\lambda) \cdot SE(\lambda) \cdot d\lambda}$$

This normalizing constant was then used to determine the expected output signal from the silicon detector by the following calculation:

A. The absolute radiometric distribution was multiplied with the absolute spectral responsivity of each of the 3 silicon detectors on a point by point basis.

B. The result was integrated from 0.4 to 1.1 μm to yield the star signal output from the detector in ampere/cm^2 of collection area.

C. The result of "B" was multiplied by $\pi/4(7.620\ cm^2)$ of collection area and by a factor of 0.8 for transmission efficiency and imaging efficiency of the optics.

D. The results of "C" were reduced to represent the following magnitude M-6 class stars:

1) +2.75 m(V)
2) +2.25 m(V)
3) +1.25 m(V)
4) +0.25 m(V)

$$Sig = K \cdot A_{lens} \cdot \eta_{trans} \cdot \frac{1}{10^{0.4}} \cdot mag \cdot \int_{0.4\mu}^{1.1\ \mu} BB(\lambda) \cdot SD(\lambda) \cdot d\lambda$$

5.6 Tabulated Results

These results are tabulated as follows:

	Predicted signal level from 3-inch dia 80% efficient optics for M-5 Star magnitudes of:			
Detector No.	+2.75 m(V)	+2.25 m(V)	+1.25 m(V)	+0.25 m(V)
1	2.6 pA	4.1 pA	10.4 pA	26 pA
2	2.5 pA	4.0 pA	10.0 pA	25 pA
3	2.3 pA	3.6 pA	9.1 pA	23 pA

5.7 SIMULATED SYSTEM TEST DESCRIPTION

The apparatus used for testing the silicon cell and preamplifier is identical to the equipment used in testing the cadmium sulfide system shown in Figure 4.1, p. 15 with the following exceptions:

1) Background illumination of the silicon cell is not required to improve the performance characteristics of the cell.

2) The hypothetical star mapper's 3-inch optical system has a transmission efficiency described by 80% of the incident energy focused in a spot of approximately 1.0 mil in diameter from 0.4 to 1.1 μm.

3) The star class used for testing silicon was M5 as opposed to A0 for testing cadmium sulfide. The reason for using an M-5 class star for silicon is the superior match between the silicon response and an M-5 (2800 °K) spectral distribution, just as an A0 (10,500 °K) spectral distribution more closely matches the cadmium sulfide response curve. An M-5 class star can be closely approximated by an unfiltered 6-volt ribbon filament lamp operated at 8 amperes. However, since the Bausch and Lomb 10-power microscope objective is not designed to be achromatic in the 0.75-μm to 1.0-μm region of the silicon spectrum, it was deemed desirable to retest to determine the size of the simulated image blur circle from 0.4 to 1.1-μm. This was found to be approximately 0.8 mil in diameter measured across the entire spatial energy distribution as seen in a Varo image converter with an S-1 photocathode. Thus the requirement on the spot diameter in exception 2 above is satisfied.

This image consequently is not only contained within the 2-mil detector slit width, but is approximately the diameter assumed for the real star image in the hypothetical image system.

The calibration procedure for the intensity of this spot is similar to the calibration procedure for the cadmium sulfide cell, and the results are:

a) The theoretical value of luminous flux for a 3.5-Mag M5 star collected by the hypothetical image system is calculated in Appendix G and equals 8.7×10^{-10} lumens.

b) The measured value of luminous flux unattenuated by neutral density filtering or spectral filtering is 2.49×10^{-7} lumens as indicated in Appendix H.

The ratio of $\frac{\text{Measured value of Luminous Flux}}{\text{Theoretical Value of Luminous Flux (3.5 Mag M5 star)}}$

is the ratio of $\frac{2.49 \times 10^{-7} \text{ lumens}}{3.771 \times 10^{-10} \text{ lumens}} = 670$

or Log ratio = 2.8.

Thus 2.8 neutral density nichrome filtering is required to properly simulate the illumination of a 3.5-Mag M5 star imaged by a high quality 3-inch diameter optical system described by 80% incident energy focused in approximately a 1-mil spot from 0.4 to 1.1 μm.

The following tests were carried out on the silicon cells No. 1, 2 and 3.

1) A uniformity scan was recorded at a 30-millisecond transit rate with a 2.75-Mag M5 class star and approximately 50 mils displacement between transits over $>$0.400 inches of the cell.

2) At a spot selected as being characteristic of the average sensitivity of the cell, the following star magnitudes were scanned at a variable high speed rate.

a. A 2.75-Mag M5 class star

b. A 2.25-Mag M5 class star

c. A 1.25-Mag M5 class star

d. A 0.25-Mag M5 class star

5.8 SIMULATED SYSTEM TEST RESULTS

5.8.1 High Speed Transits

Figures 5.17, 5.18 and 5.19 contain high speed transits with a simulated 2.75-Mag M5 star.

5.8.2 Signal

The signal level for the high speed transits in Figures 5.17, 5.18 and 5.19 are:

Detector	Signal Level from simulated 3-inch dia 80% efficient optics (Figure 4.1 modified as in Section 5.7) for M-5 Star Magnitudes of			
#	+2.75 m(v)	+2.25 m(v)	~+1.25 m(v)	+0.25 m(v)
1	2.1 picoamp	2.7 picoamp	4.1 picoamp	11 picoamp
2	1.6 picoamp	2.5 picoamp	4.3 picoamp	11.5 picoamp
3	1.8 picoamp	3.2 picoamp	3.7 picoamp	10.5 picoamp

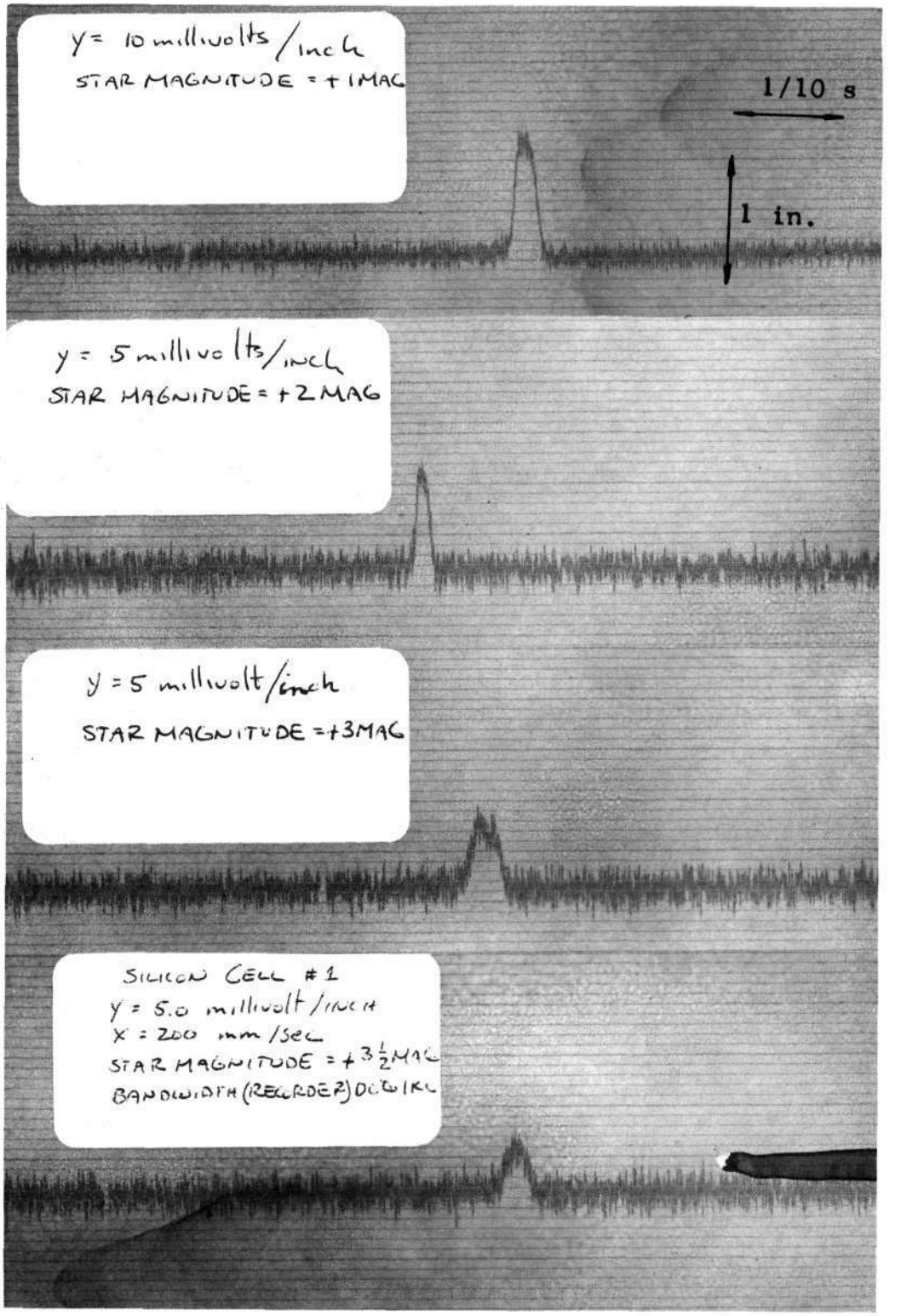

Figure 5.17 SILICON CELL NO. 1

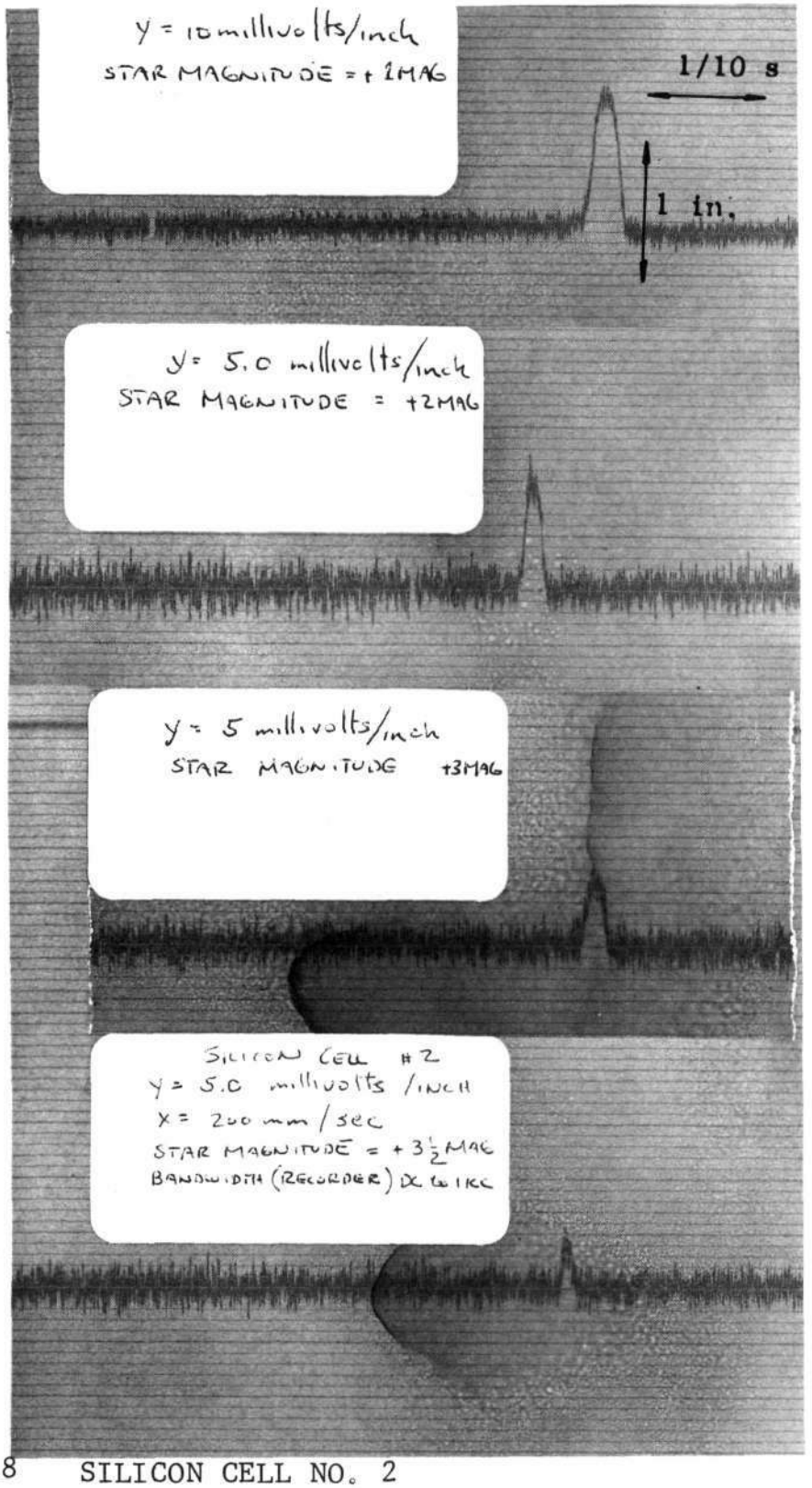

Figure 5.18 SILICON CELL NO. 2

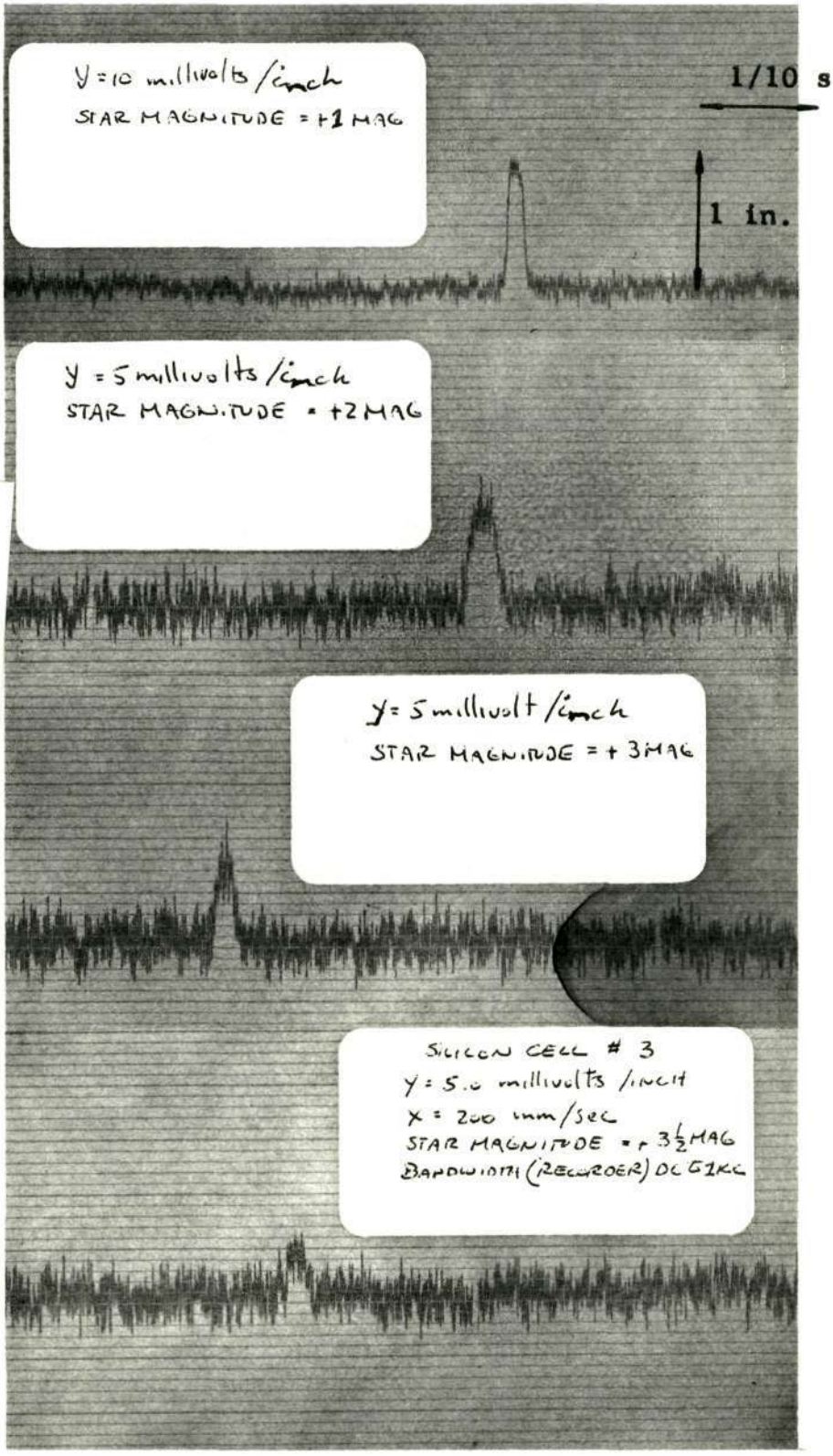

Figure 5.19 SILICON CELL NO. 3

5.8.3 Signal to Noise Ratio

The signal/rms noise ratio for these 2.75 mag star transits and a 0.5 to 550 Hz bandwidth are:

Cell No.	S/N
1	$\frac{6 \times (1.7)}{(2)} \frac{mV}{mV} = 5.1$
2	$\frac{6 \times (1.5)}{(2)} \frac{mV}{mV} = 4.5$
3	$\frac{6 \times (1.7)}{(2.75)} \frac{mV}{mV} = 3.7$

Average S/N = 4.5

No testing was done at other transit rates with silicon since the silicon response is faster than even the one-millisecond transit and the high frequency break point of the preamplifier is at 580 Hz.

5.8.4 Star Transit Pulse Shape

Figures 5.17, 5.18 and 5.19 indicate star transit pulse shape.

5.8.5 Rise Time

The rise time is a function only of transit speed for silicon within the 3 dB voltage bandwidth of the preamplifier (0.5 to 580 Hz). The rising ramp time values for cells No. 1, 2, and 3 are variable since the transit rate during the test was variable.

5.8.6 Slit Measurements

The silicon detector slits were examined under the same microscope used for cadmium sulfide. The following slit widths were measured on both ends and the middle of the slit.

Cell No.	Slit Width in Mils End-Center-End		
1	2.0	2.0	2.0
2	2.0	2.0	2.0
3	2.0	2.0	2.0

Thus the slit width is as with cadmium sulfide very accurately defined. Again, no slit deviation from a straight line was observable.

SECTION 6

CONCLUSION

6.1 CADMIUM SULFIDE DETECTOR

The cadmium sulfide detector/preamplifiers with high quality 3-inch diameter optical collection systems are capable of being utilized on +2.75 Meg star mappers with a moderate spin rate.

The predicted 10-millisecond transits of a +2.75-Mag A0 star can provide the following signal to rms noise levels, and detection probability;

HRC Cell S/N = (28/1) with a ±67% deviation from the average response for 92% of the slit transits

However, background illumination must be applied to the cells to eliminate any signal response delay due to trap-filling in the detector. This background level may be unique for any particular cell, although it appears to be optimized when the cadmium sulfide cell impedance has been lowered to between 10 and 100 megohms.

6.2 SILICON DETECTORS

The p on n silicon detectors appear to fall short of the expected noise level in the region from 0.5 to 580 Hz. These cells connected to the preamplifier exhibited noise characteristics of approximately 2 mV peak to peak. This noise value limits high speed (approximately 1-millisecond) transits of +2.75-Mag M-5 class star to a 4.5/1 signal to rms noise level.

The p on n silicon detectors, when connected directly into the same preamplifier, exhibited noise characteristics of 1.5 millivolts and thus a hard wired detector/preamplifier package could deliver approximately a 6/1 signal to rms noise level for a high speed transit of a +2.75 -Mag star. It is of importance to note that p on n detectors must be made radiation resistant either by pre-exposing them to the expected level of radiation or by sufficiently protecting them from heavy exposures of proton and

electron bombardment. This could easily be accounted for in the collection optics. Thus, the HRC silicon detector/preamplifier with a high quality 3-inch diameter optical collection system is capable of being utilized on a 2.75 -Mag star mapper with a high spin rate. The predicted 1-millisecond transits of a 2.75 -Mag M-5 class star would provide a 6/1 signal to rms noise levels and detection probabilities with a ±11% deviation from the average response for 100% of the slit transits.

APPENDIX A

SAMPLE SILICON RESISTANCE AND CAPACITANCE CALCULATION

DETECTOR #1

$$R = \left[\frac{10mV - 0.050mV}{0.050mV}\right] \left[1.0 \text{ megohm}\right] = 199 \text{ megohm}$$

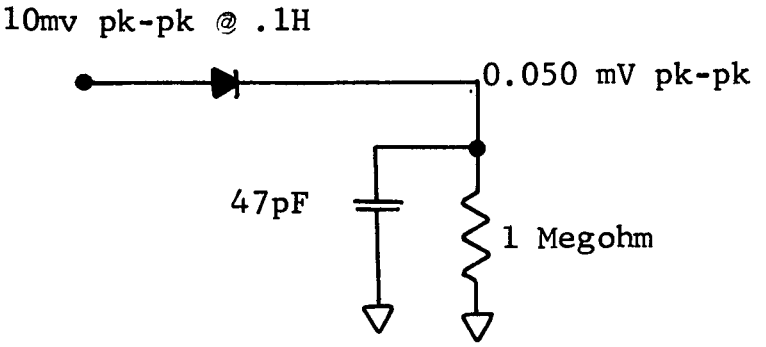

$$C = \left[\frac{4.5mV}{10mV - 4.5mV}\right] \left[377pF\right] = 308pF$$

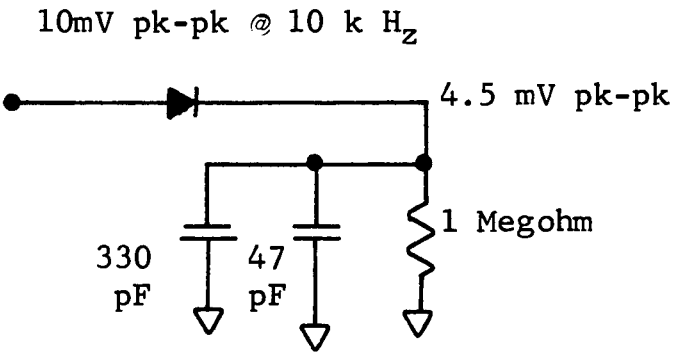

APPENDIX B

SAMPLE SILICON NOISE/ $\sqrt{HZ}$ AND NEP AND D*

Freq	At Amplifier: Output Noise pk-pk Det#1/preamp	At Amplifier: Output Noise pk-pk 330pf/preamp	At Amplifier: Output Noise pk-pk Det. only	At Preamplifier: Output Noise pk-pk Det	At Preamplifier: Input Noise pk-pk Det	At Preamplifier: Input Noise rms Det	At Preamplifier: Input Noise rms/cycle $^{1/2}$ Det
.2-.315	20 mV	5 mV	19.4 mV	14.9×10^{-5} volts	27.6×10^{-14} amp	4.6×10^{-14} amp	11.5×10^{-14} amp/$H_z^{1/2}$
.315-1.0	35	9	33.7	16.8×10^{-5}	19.5×10^{-14}	3.25×10^{-14}	4.55×10^{-14}
1.0-3.15	50	18	46.7	20.3×10^{-5}	20.3×10^{-14}	3.38×10^{-14}	2.52×10^{-14}
3.15-10	60	30	52	20.8×10^{-5}	20.8×10^{-14}	3.46×10^{-14}	1.40×10^{-14}
10-31.5	120	50	109	43.5×10^{-5}	43.5×10^{-14}	7.25×10^{-14}	1.67×10^{-14}
31.5-100	250	150	200	76.8×10^{-5}	76.8×10^{-14}	12.8×10^{-14}	1.65×10^{-14}
100-315	500	350	356	145×10^{-5}	156×10^{-14}	26.0×10^{-14}	1.88×10^{-14}
315-1k	600	525	292	116×10^{-5}	276×10^{-14}	46.0×10^{-14}	1.88×10^{-14}

$$\frac{NEP}{@\ .67\mu m,\ 200\ H_z\ c.f.,\ <-1.0mV\ Bias} = \frac{1.88\times10^{-14}\ amp/\sqrt{H_z}}{.31\ \frac{amp}{watt}} = 6.06\times10^{-14}\ watt/H_z^{1/2}$$

$$\frac{D^*}{@\ .67\ \mu m,\ 200\ H_z\ c.f.,\ <-1.0mV\ Bias} = \frac{\sqrt{2.05mil \times 510\ mil}\times\frac{2.54\ cm}{10^3\ mil}}{6.06\times10^{-14}\ watt/\sqrt{H_z}} = 1.36\times10^{12}\ \frac{cm.H_z^{1/2}}{watt}$$

APPENDIX C

Resolution Spot Size

	(50% points) Detector Width		Detector Width-- Resolution Spot Radius (80% points)	Resolution Spot Radius	Resolution Spot Diameter
.4	2.40	-	1.30	1.10	2.2
.42	2.10	-	1.50	.60	1.2
.47	2.05	-	1.50	.55	1.1
.52	2.05	-	1.15	.90	1.8
.57	2.05	-	1.20	.85	1.7
.62	2.15	-	1.50	.65	1.3
.67	1.95	-	1.25	.70	1.4
.72	2.10	-	1.20	.90	1.8
.77	2.05	-	1.40	.65	1.3
.82	2.00	-	1.40	.60	1.2
.87	2.05	-	1.50	.55	1.1
.92	2.05	-	1.35	.70	1.4
.97	2.15	-	1.3	.85	1.7
.99	2.05	-	1.2	.85	1.7
	$\overline{\text{Ave}}$ 2.05 mils				Ave = $\overline{1.5}$ mils

Rms Dev ±.10 mils

Conclusion: #1 All the energy is captured by the detector, as is evidenced by the 1.5 mils Ave resolution spot diameter.

#2 At no point does the resolution spot diameter become equal to or greater than the measured detector width.

Conclusion: #3

The detector width, does not change within the measurement error of this technique (ℓ ($\pm$0.10 mil) versus the illumination wavelength.

APPENDIX D

Sample Silicon Responsivity Calculation

DETECTOR #1

$$\bar{R}_{.77\mu m} = \frac{\left[\begin{array}{l}\text{Detector/Preamp}\\ \text{voltage output}\\ \text{at } .77\mu m\end{array}\right] \times \left[10^{-9}\ \frac{\text{Amp}}{\text{volt}}\right]}{\left[\begin{array}{l}\text{Illumination Area on the}\\ \text{Detector}\end{array}\right]} \times \frac{\left[\begin{array}{l}\text{Average Detector/Preamp}\\ \text{voltage output over the}\\ \text{entire slit at } .57\mu m\end{array}\right]}{\left[\begin{array}{l}\text{Spot Detector/Preamp}\\ \text{voltage output at } .57\mu m\end{array}\right]}}{\frac{\left[\begin{array}{l}\text{Light Mike}\\ \text{voltage output}\\ \text{at } .77\mu m\end{array}\right] \times \left[\begin{array}{l}\text{Light Mike}\\ \text{Responsivity at}\\ .77\mu m \text{ in } \frac{\text{watt}}{\text{volt}}\end{array}\right]}{\left[\begin{array}{l}\text{Illumination Area on}\\ \text{the Light Mike}\end{array}\right]}}$$

$$\bar{R}_{.77\ \mu m} = \frac{\dfrac{[240 \times 10^{-3}\ \text{volts}]\ [10^{-9}\ \frac{\text{amp}}{\text{volt}}]\ [.983]}{[\pi/4 \times (6.0\ \text{mil})^2 \times (\frac{1}{8.3})^2}}{\dfrac{[30 \times 10^{-6}\ \text{volts}]\ [\frac{1\ \text{volt}}{698\ \text{watt}}]}{[6.3\ \text{mil} \times 220\ \text{mil} \times (\frac{1}{8.3})^2]}}$$

$$\bar{R}_{.77\ \mu m} = 0.27\ \frac{\text{amp}}{\text{watt}}$$

APPENDIX E

PREDICTED POWER INCIDENT ON DETECTOR

Assume AVE 6th Mag (Ko) star at the earth's surface

The illumination (I) of a 6th Mag star is

$$I_{6th\ Mag} = 8.3 \times 10^{-9} \frac{lumen^*}{m^2} = 7.7 \times 10^{-10} \frac{lumen}{ft^2}$$

$$I_{3.5th\ Mag} = 7.7 \times 10^{-10} \times 10 \frac{lumen}{ft^2}$$

$$= 7.7 \times 10^{-10} \times 9.9$$

$$= 7.7 \times 10^{-9} \frac{lumen}{ft^2} \text{ at the earth's surface}$$

$$= 7.7 \times 10^{-9} \frac{lumen}{ft^2} \times \frac{4.66\ 0Mag\ in\ space\ for\ A0\ class^{**}}{3.45\ 0Mag\ at\ Earth\ surface\ for\ A0\ class} = 1.04 \times 10^{-8} \frac{lumen}{ft^2}$$

Then the luminous flux (P) present at the spot is

$$P_{Det} = I_{3.5th\ Mag} \times Area_{Collection} \times \tau_{Collection}$$

$$= 10.4 \times 10^{-9} \frac{lumen}{ft^2} \times \frac{1}{144} \times \frac{ft^2}{in^2} \times \frac{\pi}{4} 3^2\ in^2 \times .8$$

$$P_{Det} = 4.1 \times 10^{-10} \text{ lumen in space}$$

---

*Optical Engineering Handbook Electro-Optical Engineering Unit G.E. Ordinance Department. Scranton Operation, Dr. J. A. Mauro Editor and Co-Author.

**SPARS Stury Program

APPENDIX F

MEASURED POWER INCIDENT ON DETECTOR (Ao STAR FILTER FROM 0.4 to .75 μm)

The luminous flux (P) present at the detector plane as measured by the Spectra Prichard Photometer, indicated in Figure 4.1 and 4.2 is

$$P_{Det} = \frac{B}{\pi} \times \frac{\pi}{4} \alpha^2 \times A \times \frac{1}{\tau_{\text{microspectar lens}}} \times \frac{1}{\tau_{\text{mirror}}}$$

The following definitions apply B is the spot brightness in Ft lamberts as measured by the SPECTRA Prichard Photometer where the image of the spot of light at the detector plane as seen in the photometer is entirely contained within the angular field of view aperture of the Photometer.

α is the angular field of view aperture of the Spectra Prichard Photometer.

A is the collection area of the SPECTRA Prichard Photometer collection lense.

$$= \frac{.017 \text{ ft lamb.}}{\pi} \times \frac{\pi}{4} (.01745)^2 \times A \times \frac{1}{\tau_{M.S.}} \times \frac{1}{\tau_M}$$

$$= .13 \times 10^{-5} \frac{\text{lumen}}{\text{ft}^2} \times \frac{1}{144} \frac{\text{ft}^2}{\text{in.}^2} \times \frac{\pi}{4} (2 \text{ in.})^2 \times \frac{1}{\tau_{MS}} \times \frac{1}{\tau_M}$$

$$= .09 \times 10^{-7} \frac{\text{lumen}}{\text{in.}^2} \times \pi \text{ in}^2 \times \frac{1}{.9} \times \frac{1}{.9}$$

$$P_{Det} = .283 \times 10^{-7} \text{ lumen} \times \frac{1}{.81}$$

$$P_{Det} = 3.5 \times 10^{-8} \text{ lumens}$$

τ_{mirror} is the total transmission efficiency of the mirror inserted in the optical path to permit the measurement of the luminors flux at the equivalent detector plane.

$\tau_{microspectar\ lens}$ is the total transmission efficiency of the auxilliary lens (SPECTRA MICROSPECTAR) necessary to collect all the energy coming from thie equivalent detector plane.

APPENDIX G

PREDICTED POWER INCIDENT ON DETECTOR

Assuming AVE 6th Mag (Ko) star, the illumination (I) is

$$I_{6th\ Mag} = 7.7 \times 10^{-10} \frac{lumen}{ft^2}$$

$$I_{3.5th\ Mag} = 7.7 \times 10^{-9} \frac{lumen}{ft^2} \quad \text{at earth's surface}$$

$$= 7.7 \times 10^{-9} \frac{lumen}{ft^2} \times \frac{11.18\ 0Mag\ MO\ class\ star\ in\ space}{9.09\ 0Mag\ MO\ class\ star\ at\ Earth\ surface} * = .945 \times 10^{-8} \frac{lumen}{ft^2}$$

Then the luminous flux (P) present at the spot is

$$P_{Det} = I_{3.5th\ Mag} \times A_{Collection} \times \tau_{Collection}$$

$$P_{Det} = 9.45 \times 10^{-9} \frac{lumen}{ft^2} \times \frac{1}{144} \frac{ft^2}{in^2} \times \frac{\pi}{4} 3^2\ in.^2 \times .8$$

$$P_{Det} = 3.71 \times 10^{-10}\ \text{lumens in space}$$

*SPARS Study Program - Wright-Patterson AFB

APPENDIX H

MEASURED POWER INCIDENT ON DETECTOR (NO FILTERING) (M-5 STAR FROM 0.4 TO 1.1 μm)

The luminous flux (P) present at the detector plane as measured by the spectra Prichard Photometer, indicated in Figure 4.1 and 4.2 is

$$P_{Det} = \frac{B}{\pi} \times \frac{\pi}{4} \alpha^2 \times A \times \frac{1}{\tau_{microspectar}} \times \frac{}{\tau_{mirror}}$$

The definition of B, α, A, $\tau_{microspectar}$ and τ_{mirror} are identical to those definition found in Appendix F.

$$P_{Det} = \frac{.125 \text{ ft. Lamb.}}{\pi} \times \frac{\pi}{4} (.01745)^2 \times A \times \frac{1}{\tau_{MS}} \times \frac{1}{\tau_{M}}$$

$$P_{Det} = (.925 \times 10^{-5} \frac{\text{lumen}}{ft^2}) \times \frac{1}{144} \frac{ft^2}{in^2} \times \frac{\pi}{4} (2 \text{ in})^2 \times \frac{1}{.9} \times \frac{1}{.9}$$

$$P_{Det} = 2.02 \times 10^{-7} \text{ lumens} \times \frac{1}{.81}$$

$$P_{Det} = 2.49 \times 10^{-7} \text{ lumens}$$